INTERNATIONAL ATOMIC ENERGY AGENCY
UNITED NATIONS EDUCATIONAL, SCIENTIFIC AND CULTURAL ORGANIZATION

INTERNATIONAL CENTRE FOR THEORETICAL PHYSICS
34100 TRIESTE (ITALY) - P.O.B. 586 - MIRAMARE - STRADA COSTIERA 11 - TELEPHONE: 2240-1
CABLE: CENTRATOM - TELEX 460392-1

SMR/406-17

THIRD AUTUMN WORKSHOP ON ATMOSPHERIC
RADIATION AND CLOUD PHYSICS
27 November - 15 December 1989

"Parameterization of Cloud and Radiation Interactions
in General Circulation Models"

Y. FOUQUART
Laboratoire d'Optique Atmosphérique
Université de Lille
Villeneuve d'Ascq
FRANCE

Please note: These are preliminary notes intended for internal distribution only.

PARAMETERIZATION OF CLOUDS AND RADIATION INTERACTIONS IN GENERAL CIRCULATION MODELS

Y. Fouquart

Laboratoire d'Optique Atmosphérique, Université de Lille

Villeneuve d'Ascq, France

1 Introduction

In this course, it must have already been stressed that clouds and radiation interactions are one of the key problem in understanding the climate, its natural variability and its sensitivity to natural or anthropogenic forcings. According to Webster and Stephens (1984) "of all climate parameters, clouds have the largest potential effect on the radiation field".

The effect of clouds on the earth radiation budget

The effect of clouds on the radiation budget at the top of the atmosphere is twofold: (i) in the shortwave, clouds are very efficient at reflecting the incident solar radiation back to space. They, thus, decrease the amount of solar energy available for absorption in the atmospheric column and at the surface, (ii) in the longwave, they absorb the infrared radiation emitted by the surface and the lower atmosphere and re-radiate to space at colder temperatures, thus producing a heating effect. The balance between these two compensating effects depends on a variety of conditions such as the regional distribution of cloud types and cloud characteristics and its seasonal variation.

Both effects are large, therefore it is not surprising to find considerable desagreements in satellite estimates of climate sensitivity to cloudiness. This sensitivity was first analysed in some details by Schneider (1972), who considered the sensitivity of the radiation balance R_N to cloud cover fraction A_c, in terms of a sensitivity parameter $\gamma = \partial R_N / \partial A_c$. Here R_N is the net radiation balance at the top of the atmosphere; it is thus the difference between the absorbed solar energy and the outgoing terrestrial radiation.

Since then, there have been many attempts to determine γ from satellite observations (Cess, 1976; Ellis, 1978, Ohring and Clapp,1980; Hartmann and Short, 1980). The results ranged from near cancellation of albedo and greenhouse effects ($\gamma \simeq 0$) to strong albedo dominant effect ($\gamma \simeq -80 Wm^{-2}$). Indeed,to determine γ, one has to isolate variations of R_N which are uniquely due to cloud cover variations, this is practically very difficult if not impossible with purely observationnal techniques.

More recently, Charlock and Ramanathan (1985) proposed that one approachs this problem by first examining the "cloud radiative forcing" which is defined as the difference $R_N - R_N^{clear}$ where R_N^{clear} applies to clear-sky conditions and R_N applies to overall (clear plus cloudy) conditions.

From the point of view of observation, it appears easier to determine the cloud radiative forcing from the difference between overall mean irradiances and the mean clear-sky irradiances, rather than from the determination of cloud fraction, and cloud parameters such as cloud albedo, cloud height, cloud top temperature and emittance (Hartmann et al, 1986; Ramanathan et al, 1989). This implicitely assumes that atmospheric conditions in the clear-sky areas that are found do not differ systematically from average atmospheric conditions over the region considered; this may not always be so. Nevertheless, the availability of regional estimates of clear-sky irradiances in the processed data of the Earth Radiation Budget Experiment (ERBE: Barkstrom, 1984)

allows an empirical estimate of the cloud radiative forcing. From the data available for the month of April 1985, Ramanathan et al (1989a) found a global shortwave cloud forcing of -44.5 Wm^{-2} and a longwave forcing of 31.3 Wm^{-2}. The net effect is thus a cooling one (-13.2 Wm^{-2}). For the month of July 1985, Ramanathan et al (1989b) also concluded to a net cooling effect of clouds (16.6 Wm^{-2}).

In what sense is that a cooling? If we consider the present equilibrium climate with clouds, then the cloud radiative forcing is the negative of the forcing that would apply in the event of instantaneous removal of the cloud opacity. According to ERBE observations, rendering the clouds transparent would produce an initial heating of roughly $15 Wm^{-2}$. This sort of experiment is easy to carry out in model simulations.

Climate models exhibit considerable desagreement regarding the magnitude of shortwave and longwave cloud forcings terms, and even the sign of the net forcing is not certain, although most results are negative, between 0 and -40 Wm^{-2} (Cess and Potter, 1987; Cess et al, 1989). The use of cloud radiative forcing then reveals extremely clearly the inadequacy of current treatments of clouds in climate models. It should be noted that accurate determination of cloud radiative forcing is only the first step to evaluate climate-cloud-radiation feedback this cloud feedback includes the reaction of cloud cover and cloud characteristics in response to climate forcing. It is then hardly surprising that there should be a fairly wide range of predictions of sensitivity of the climate to doubling atmospheric CO_2. The model comparisons (Cess et al, 1989) show that the major source of uncertainty is in the treatment of cloud-radiation interactions.

The effect of clouds on the surface radiation budget

The surface radiation budget (SRB) is intimately related with the nonradiative surface-to-atmosphere energy (sensible and latent heat) fluxes, which govern in particular the surface temperature. Except in polar regions, the downward shortwave radiation is always strongly diurnally varying, and it is often the driver of the boundary layer activity as well as deep convection; its amount and spectral composition determines the the energy available for photosynthesis. Cloud cover always has a strong influence on the downward shortwave radiation. This, together with the reasonable assumption that atmospheric absorption usually plays a secondary role, is the basis of most algorithms for the derivation of the shortwave downward irradiance from satellite observations: the variations of absorption or scattering by the other radiatively active components of the atmosphere can be fixed at climatological values or parameterized as they are small compared to the cloud influence.

Cloud cover also has a strong influence on the downward longwave irradiance, even though in this case, clouds act to decouple the surface from space (Stephens and Webster, 1984). Using climatological temperatures and humidity profiles, Chou (1985) estimated the sensitivity of the SRB over the tropical Pacific ocean to different atmospheric parameters. He considered uniform increases of the air temperature ($1K$), specific humidity (15%), or cloud top pressure ($66\ mb$); he obtained changes of, respectively, roughly 5 Wm^{-2}, 7 to 11 Wm^{-2}, and 1.8 to 2.4 Wm^{-2}. As for the cloud cover, a 5% increase gives a decrease of the surface net irradiance of 8 to 10 Wm^{-2} whereas a 20% increase of the cloud optical thickness results in a decrease of 4 to

5 Wm^{-2}. This confirms the dramatic influence of clouds in the shortwave, whereas for the tropical areas Chou considered, the net longwave irradiance is mostly sensitive to humidity. Outside the tropics, the effect of cloud cover on the longwave is much stronger, manifesting itself for example in the well-known differences in night time minimum temperatures between clear and cloudy conditions.

As stressed by Woods (1984) and Webster and Stephens (1984), the efficiency of solar radiation to heating the oceanic mixed layer is strongly dependent on its spectral distribution. The blue-green sunlight can sometimes reach deeper than 100 m, whereas the red light is absorbed in a few meters and the infrared in a few millimeters. Therefore, it is not sufficient to consider the global impact of clouds on the SRB. Variations in the cloud cover or cloud types by affecting not only the global SRB but also its spectral distribution may significantly impact the structure of the ocean mixed layer.

The effect of clouds on the diabatic heating of the atmosphere

Through their impact on the longwave radiative cooling, clouds also have the potential of a significant impact on the dynamics of the atmosphere. Albrecht and Cox (1975) were the first to suggest that differential radiative heatings caused by the contrasts between clear and cloudy regions could play an important role in determining the amplitude and the structure of tropical waves. Webster and Stephens (1984) compared the vertical distribution of the various components of the diabatic heating and its variation with latitude or longitude. They showed very clearly that (i) the radiative heating is a very important component, sometimes predominant, of the total diabatic heating and (ii) that it has very strong longitudinal variations mainly attributable to variations in water vapor and clouds. Byrd and Cox (1984) analysed a tropical cloud cluster system observed during the GATE experiment; they estimated the amplitude of the differential radiation heating and found that its maximum was located in the mid troposphere at the beginning of the life of the system with typical values up to 1.3 to 3.4 $K.d^{-1}$ over a 110 km distance. Using a simple model of vertical motion, they found that these strong contrasts result in a very significant radiatively driven circulation around the cloud system at its earlier stages, with subsidence in cloud free regions and convergence in the lower levels of the cloud area, thus intensifying the convective activity.

The effect of clouds in climate models

Since the role played by the interactions between clouds and radiation is so important in various processes of the climate system, it is of prime importance that they are adequately taken into account in 3D models. As a matter of fact, simulations of the effect of doubling atmospheric CO_2 concentration have shown a very large sensitivity to cloud radiative effect (Schlesinger and Mitchell, 1986) : estimates of the surface temperature changes using models with fixed cloud cover give increases close to 2 K whereas those obtained using interactive clouds range between 4 and 5 K. In these experiments, however, the cloud optical properties remain constant. Somerville and Remer (1984) suggested that variations of the optical properties might

significantly reduce the climate sensitivity to the increase in greenhouse gases. More recently, Mitchell et al (1989) suggested that the phase of the condensed water could induce a strong negative feedback. On the other hand, Cess et al (1989) showed that very large differences in model responses to identical forcings correlated very well with the model "cloud forcings". The treatment of clouds and radiation interactions in climate models is thus still a critical problem for a proper simulation of climate scenarios.

So far, despite of this drastic influence on the climate system, the treatment of clouds and radiation interactions has often been very crude in many General Circulation Models (GCMs). In particular, the cloud characteristics are tuned to assure the long term equilibrium of the model or/and to fit some spatial observations (Geleyn et al, 1982), but this tuning is itself dependent on so many characteristics of the model (in particular, on the cloud generation scheme, convection, etc.) that there is no evidence that the effect of clouds on the radiation field is realistic. Buriez et al (1988) have shown that, on the contrary, this tuning procedure could result in strongly biased cloud optical properties that compensate underestimated cloud covers. In many cases, the longwave and shortwave properties have been tuned independently and in the first generation of GCMs, clouds were simply assumed to be black in the infrared. In the near future, however, clouds are going to be more and more interactive with the rest of the model and the liquid water content is already a pronostic variable in some GCMs (Sundqvist, 1978; Le Treut and Li, 1988). This is this perspective that we consider in this paper.

An adequate simulation of the interactions between clouds and radiation also requires that attention be given to the effect of radiation on cloud dynamics. Particularly important in that context is the role of radiative divergence on the entrainment processes in low-level clouds (Deardorff, 1976; Randall et al, 1984, among others) and the role of the cloud shortwave absorption (Fravalo et al, 1981; Hanson and Gruber, 1982; Bougeault, 1985). For this purpose, the profiles of the radiation divergence within the cloud need to be known accurately.

In the context of the above discussion, the purpose of this paper is to review various aspects of the effect of clouds on radiation, both from an experimental and a theoretical point of view and to suggest a parameterization of cloud optical properties which allows a realistic representation of their effect on both shortwave and longwave irradiances and radiation divergences. Considering the observations available so far, the review is mostly focused on low and sometimes mid level clouds for which a good deal of data is available including simultaneous microphysical and radiative observations. This lack of data on high level clouds should be filled in with the availability of the results of the First ISSCP Regional Experiment-Cirrus (FIRE) (Starr, 1987) and the International Cirrus Experiment (ICE) (Raschke and Rockwitz, 1988).

2 Clouds generation in General Circulation Models

In the actual atmosphere, clouds are interactively linked to dynamical, hydrological,turbulent and radiative processes over scales ranging from the microphysics of cloud particles to the planetary scale impact of extended decks of stratiform clouds. In the present atmospheric general circulation models, clouds are not related to the hydrological cycle; they exist only for their direct impact on the radiation field and their characteristics (horizontal cover, height, optical

properties) are either fixed or diagnosed from a limited set of parameters (for a review, see Rutledge and Schlesinger, 1985). The radiative effect of clouds depends on their horizontal extension (the cloud cover A_c defined as the fraction of the model grid filled with clouds), their height and their optical characteristics which will be addressed in section 3 and 4. In this section we examine how these quantities are determined in GCMs.

Parameterization of the cloud fraction

Following [illegible]orinsky (1960), most modelers have relied on resolvable-scale relative humidity for diagnosing nonconvective cloudiness. The first parameterizations were linear, however many authors used more complicated relations. Geleyn et al. (1982) linked the horizontal cloud cover A_c to the relative humidity through a quadratic relationship

$$A_c = \left(max \left(0, \frac{RH - RH_c}{1 - RH_c} \right) \right)^2 \qquad (1)$$

where RH_c is a critical relative humidity defined as a function of the sigma pressure (σ =pressure/surface pressure).

Relating clouds and relative humidity is certanly quite reasonnable; however the relation is far from being clear in terms of model variables. A look at the sky is sufficient to see that clouds present a spatial variability at a scale much smaller than that of a model grid.

An example

The work of Buriez et al. (1988) provides a good example of this problem. Over the area outlined in Figure 1, they constituted a data file containing, for a one-year period between 1 February 1982 and 31 January 1983, analyzed large-scale fields of geopotential height, temperature, humidity and wind collocated with satellite measured radiances and cloud parameters derived from these measurements.

The large-scale fields were derived from the 4-dimensional assimilation of observation data carried out routinely with the ECMWF forecasting system. The ECMWF operational system is an intermittent data assimilation system (data are assimilated with a frequency of 6 hours) consisting of a multivariate optimum interpolation analysis, a non-linear normal mode initialization and a a first guess forecast. A complete description of the data assimilation system can be found in Lorenc (1981). The analysed large scale fields were stored at the resolution of the ECMWF model. Thus, the studied area included a total of 1189 grids of size $(1.875^o)^2$. In each of them, clouds parameters were also stored once every 24 hours. These parameters were derived from AVHRR measurements (Advanced Very High Resolution Radiometer on board of NOAA satellites). The method which was developped by Phulpin et al. (1983), used a two-dimensionnal (visible viz infrared) technique to estimate fractional cloud covers over the ocean and to classify the cloudiness in five levels (plus one for the surface).

In Figure 2 are only considered clouds which top is below 800 mb according to the IR

chanels. For this particular subset (1436 cases), were only considered the situations with no above that level in ECMWF grids. The figure presents the satellite derived cloud cover as a function of the analysed relative humidity in the layer (1000-800mb). The solid curves represent the result of the correlations $A_c = f(R_H)$ and $RH = f(A_c)$ respectively. The dispersion is typical of this sort of attempt (J. Slingo, private comunication) and is related to the high spatial variability of humidity. At a scale small enough to represent individual clouds, 100% relative humidity should certainly be a good criteria for cloud formation, the problem is that at the same scale 99% means no cloud. Horizontal and vertical spatial integration of humidity leads to an almost complete lost of information.

Nevertheless, a statistical analysis performed over a large subset (Heinburger and Royer, private communication) concluded that relative humidity remained the best predictor of cloudiness, at least for this particular climatic region in which convective clouds are not predominant. (see Table 1)

More complex parameterizations

In addition to relative humidity many schemes used other model prognosticated quantities. The basic idea is that the spatial variations of the relative humidity are themselves related to other dynamical or thermodynamical (temperature) characteristics of the atmosphere. Figure 3, still from Buriez et al (1988) illustrates this possiblity. For the same cases as in Figure 2, Figure 3 shows the dependence of the cloud cover upon the potential temperature difference ($\Delta\theta$) in the 800-950 mb layer. The dispersion remains very large, but the correlation is now much more significant and the root mean square error for a larger subset of 2866 cases is 0.34 to be compared with 0.41 with the original Geleyn's parameterization. In addition, the original formulation presented a bias (-0.18) completely eliminated in that case.

Following Sasamori's (1975) assumption that clouds are generated by vertical motions of air parcel originating independantly from different depths, Hense and Heise (1984) have developped a completely different scheme in which the cloud cover is linked to the horizontal variance of the model vertical velocities.

For the ECMWF operationnal model, Slingo (1987) developped a scheme which distinguishes convective, high, middle and low-level clouds. In this scheme, convective cloud cover is determined from the scaled time averaged precipitation rate (P) from the model convection scheme

$$A_c = a + b \log P \qquad (2)$$

provided that convection extends above 400 mb and the convective cloudiness exceeds 40%. A part of the high cloud cover is linked to convective clouds

$$A_H = 2.0(A_c - 0.3), \qquad (3)$$

whereas extratropical and frontal cirrus are determined according to the Geleyn's parameterization (see relation 1). Middle level clouds are also parameterized according to relation (1); however to allow for the the dry subgrid scale downdraughts in the environnement of the cloud, RH is replaced by

$$RH_c - RH(1 - A_c). \qquad (4)$$

Low level clouds were divided in two categories:

(1) those associated with extratropical fronts and tropical disturbances for which the Geleyn's formula (4) still applies with a condition of no subsidence (vertical velocity ω must be negative) and a linear transition to this case:

$$A'_L = \left(max\left(0, \frac{RH - RH_c}{1 - RH_c}\right)\right)^2 \tag{5}$$

and

$$A_L = \begin{cases} A'_L(1 - 10.0\omega) & \text{for } -0.1 < \omega \leq 0 \\ A'_L & \text{for } \omega \leq -0.1 \\ 0 & \text{for } \omega > 0 \end{cases} \tag{6}$$

(2) those linked with the boundary layer and associated with low-level inversions in temperature and humidity. For those clouds, the cloud cover was related to the lapse rate of the most stable layer below 750mb.

$$A_L = -6.67\left(\frac{\Delta\theta}{\Delta p}\right)_{min} - 0.667. \tag{7}$$

In addition, to prevent clouds forming under dry inversions such as those over deserts and the winter pole, a dependence on the relative humidity at the base of the inversion (RH_{base}) is introduced:

$$A_L = \begin{cases} 0 & \text{if} RH_{base} < 0.6 \\ A'_L(1.0 - (0.8 - RH_{base})/0.2) & \text{for } 0.6 \leq RH_{base} < 0.8 \\ A'_L & \text{otherwise} \end{cases} \tag{8}$$

For the UCLA GCM, Randall et al. (1985) developped a boundary layer model in which the PBL depth is a prognostic variable. Thus, a stratocumulus cloud is assumed to occur whenever the upper portion of the PBL becomes saturated provided that cloud top entrainment does not occur. The thickness of the cloud is determined by the PBl depth (cloud top) and the condensation level (cloud base).

Recently, Harshvardan et al. (1989) modified this last generation scheme: stratocumulus cloud cover is assumed to be $A_L = 1$ when they are more than 12.5 mb thick, and decreases linearly for thinner clouds. Convective clouds are assumed to have negligible cloud cover below 400 mb, above, an optically thick "anvil" cloud is assumed to horizontally fill the grid column, from 400mb to the highest level reached by the convection. Supersaturation clouds occur when the relative humidity equals or exceeds 100%, they are assumed to have a cloud fraction of 1 and to vertically fill their GCM layer.

According to Slingo (1987), these diagnostic schemes have reached a reasonnably successfull level where cloud distributions compare favorably with satellite data. However, this agreement is essentially qualitative and a rigorous quantitative test is still missing to evaluate cloud generation schemes.

Buriez et al (1988) used their data file to compare model generated and observed (satellite derived) cloud covers. To attenuate the effect of the uncertainties linked to the estimate of the

cloud top pressure, they compared the profiles of the cumulative cloud covers ($A(p)$) defined as the toal percent of cloudy sky with cloud top pressures lower than p. Therefore, they combined the model generated clouds assuming random overlap to simulate the satellite signal. Figure 4 compares these cumulative cloud covers. The model generated cloudiness is strongly underestimated ($A_c^{model} = 0.34, A_c^{observed} = 0.60$) and most of the desagreement comes from the around 800 to 900 mb. To prevent unrealistic cooling by permanent clouds appearing in the lower layers, an ad-hoc θ filter was applied in the ECMWF model at this time: no cloud was allowed in the boundary layer when the potential temperature was lower than at the surface for the layers in question and all layers underneath. Removing this filter considerably increases the total cloud cover (up to $A_c = 0.56$) but the desagreement at the 850 mb level remained mostly unchanged.

Since then, the ECMWF cloud generation scheme has been changed and a shallow convection scheme was introduced which allows the moistening of the free troposphere above the boundary layer; this should have strongy improved the cloud generation just above 850 mb. The availability of the data from the International Satellite Cloud Climatology project (ISCCP, Schiffer and Rossow, 1985) should facilitate much deeper quantitative comparisons.

Parameterization of cloud optical characteristics

The radiative effect of clouds, also depends on their optical properties. However, as noted in the introduction, the characterization of the cloud optical properties in GCMs is generally very crude and in most cases, they are tuned to assure the long term equilibrium of the model. At best, they are tuned to fit some (non exhaustive) set of spatial observations. A consequence is that until recently, in many models, the shortwave and longwave properties (to be discussed in the following sections) were adjusted independantly and were not consistent between each other.

In the ECMWF model, the longwave and shortwave optical properties are both calculated from a liquid water content in a way similar to that proposed in the following sections. The water content itself is proportionnal to the saturation specific humidity of the layer in which the clouds occur; the proportionnality coefficient is γ. In the original scheme (Geleyn et al., 1982), γ was set to 0.2%.

The importance of the role played by these characteristics is illustrated in Table 2. In this table, are reproduced the components of the observed and calculated radiation budgets at the top of the atmosphere for the region and the period investigated by Buriez et al. The calculations have been performed in such a way as to minimize the causes of errors which could result from the spectral characteristics of AVHRR, that is: the components of the radiation budget (absorbed solar energy$Q$ and outgoing longwave radiation F) have been calculated on the spectral bandpaths of the AVHRR chanels.

Let R_N^* and $\overline{R_N}$ be the averaged observed and computed radiation budgetsrespectively. The difference between those two quantities is significant ($R_N^* - R_N = 7\ W.m^{-2}$) but small given the large difference between the observed and computed cloud covers ($A_c^* - \overline{A_c} = 0.26$). To explain this fact, we first determine the fraction of $\overline{R_N^*} - \overline{R_N}$ actually linked to the difference $A_c^* - \overline{A_c}$. Let us assume, as in Ellis (1978), that, on the average, the radiation budget is a linear

function of the cloud cover, i.e.,

$$R_N \quad R_{N\mathbf{clear}} + \frac{\partial R_N}{\partial A_c} A_c \,, \tag{9}$$

where $R_{N\mathbf{clear}}$ is the averaged radiation budget observed in clear-sky, otherwise identical atmospheric conditions; therefore, $\frac{\partial R_N}{\partial A_c}$ is a partial derivative. If, similarly,

$$R_N^* \quad R_{N\mathbf{clear}}^* + \frac{\partial R_N^*}{\partial A_c^*} A_c^* \,, \tag{10}$$

Equations (9) and (10) give

$$R_N^* - \overline{R_N} \quad R_{N\mathbf{clear}}^* \quad R_{N\mathbf{clear}} + \frac{\partial R_N}{\partial A_c}\left(A_c^* \quad \overline{A_c}\right) + \left(\frac{\partial R_N^*}{\partial A_c^*} - \frac{\partial R_N}{\partial A_c}\right) A_c^* \,. \tag{11}$$

In (11), the first r.h.s. term corresponds to the difference between the computed and observed radiation budgets in clear-sky conditions. This difference was found to be negligible provided a slight temperature adjustement is made on the sea surface temperature. The second r.h.s. term in (11) is due to the actual difference between the cloud covers assuming the same optical properti[illegible] for both the observed and the computed clouds. The third r.h.s. term is linked to the differences between the optical properties of the clouds; it would appear even if the observed and computed cloud covers were identical.
$\frac{\partial R_N^*}{\partial A_c^*}$ and $\frac{\partial R_N}{\partial A_c}$ are determined for the data set from (10) and (9) respectively; their values are presented in Table 2, and

$$\frac{\partial R_N}{\partial N}\left(A_c^* - \overline{A_c}\right) = +15\ W.m^{-2}$$

and

$$\left(\frac{\partial R_N^*}{\partial A_c^*} - \frac{\partial R_N}{\partial A_c}\right).N\overline{A_c}^* = -8\ W.m^{-2}\,.$$

In other words, the averaged difference $R_N^* - \overline{R_N}$ is 7 $W.m^{-2}$, but is actually twice that much when the compensating effect linked to the differences in cloud optical properties is excluded.

These differences in the optical properties of the observed and computed clouds are displayed in both the shortwave and the longwave ranges: the generated clouds reflect too much in the shortwave range ($\frac{\partial Q^*}{\partial A_c^*} - \frac{\partial Q}{\partial A_c} = -15\ W.m^{-2}$) and have too small an emissivity in the longwave range ($\frac{\partial F^*}{\partial A_c^*} - \frac{\partial F}{\partial A_c} = +10\ W.m^{-2}$) thus giving the total difference ($\frac{\partial R_N^*}{\partial A_c^*} - \frac{\partial R_N}{\partial A_c} = -25\ W.m^{-2}$). A more detailed examination shows that the too large brightness temperature of the generated clouds is not due to too low clouds, but to too transparent high clouds.

This example exemplifies the role of the cloud optical characteristics: in the present case an efficient tuning of these characteristics through the adjustment of γ has strongly compensated the discrepancies between observed and generated cloud covers. This is one more example of how to get good results for the wrong reasons. With the recent change of the radiation codes in the ECMWF model, the γ coefficient has been readjusted and a validation based on the utilisation of both ISCCP and ERBE data has been carried out (Morcrette, personnal communication).

More recently Harshvardan et al, (1989) linked the cloud optical properties to the cloud temperature T_C and the cloud thickness Δp_C. These authors parameterized the shortwave

optical thickness (δ: see section 3) and related the infrared emissivity ϵ to this quantity; this is very similar to parameterizing the liquid water content:

$$\delta = \begin{cases} a(T_c - T_0)^2 & \text{if } T_0 \le T_C \le -10°C \\ b\Delta p_c & \text{for } T_C \ge 0°C \end{cases} \tag{16}$$

with a linear interpolation between $-10°C$ and $0°C$. T_0 is a critical temperature : $T_0 = -82.5°C$. They use $a = 2.0 * 10^{-6}$ and $b = 0.08$ (Δp_C is in mb). The IR emissivity is linked to δ through $\epsilon = 1 - \exp(-0.75\delta)$.

The major disadvantage of the diagnostic methods is that clouds are passive and do not interact with the rest of the model: in other words they exist for their radiative effect but have no influence on latent heat release in the atmosphere neither on precipitations. As noted by Slingo (1987) another disadvantage is that these schemes are not easily transferable from a model to another one since they are so strongly dependent on the other model parameterizations, either explicitely or implicitely.

A more physical approach has been initiated by Sundqvist (1978) followed by a number of groups (Smith and Pearson, 1986; Roeckner and Schlese, 1985; Le Treut and Li, 1987). In this approach, the cloud water is an additionnal prognostic variable and is explicitely calculated through an equation of evolution. Despite of difficulties in closure assumptions, this method seems very promising as illustrated by Le Treut and Li (1987) who compared cloud covers generated by the Laboratoire de Meteorologie Dynamique (LMD) GCM using this prognostic method to the ISCCP derived cloud covers.

In the following sections, we keep the point of view that soon, GCMs will follow that way and include cloud water as a prognostic variable. We, thus,consider the problem of parameterizing cloud optical properties in terms of of cloud water.

3 The influence of clouds on the shortwave radiation

The cloud efficiency at reflecting the solar radiation and reducing the solar energy available at the surface depends on a variety of parameters which concern the cloud itself (inherent parameters) and on a variety of external conditions such as direction of insolation, surface reflectivity, etc. The inherent cloud parameters are frequency dependent, they are:

1. the optical thickness δ_ν which characterizes the attenuation of the direct solar beam due to both absorption and scattering,
2. the single scattering albedo ω_ν which is the probability that a photon is scattered when interacting (by scattering or absorption) with a particle,
3. the scattering phase function $p_\nu(\mathbf{s}, \mathbf{s}')$ which gives the probability of a photon to be scattered in the direction $\mathbf{s}'$ when incident in direction $\mathbf{s}$.

3.1 Cloud layer reflectances and transmittances

For space borne observations of clouds, the complete dependence of the radiance on the geometry must be accounted for. This dependence is one of the major problems in cloud remote sensing. In this paper, however, we consider the effect of clouds on the radiation field from the climatic perspective; we are thus more interested by irradiances (Wm^{-2}) than radiances($Wm^{-2}sr^{-1}$). Approximate methods have been developed to achieve a quick solution to the radiative transfer equation by decomposing the radiation field into two opposing streams. In these methods, the scattering phase function is reduced to its first moment, the asymmetry factor

$$g_\nu = \frac{1}{2}\int_{-1}^{+1} p_\nu(\Theta)\cos\Theta\, d(\cos\Theta), \tag{17}$$

where $\Theta = (s, s')$ is the scattering angle.
According to King and Harshvardan [1986], such approximate irradiance computations are generally accurate within a few percent.
In these conditions, the inherent cloud optical properties reduce to three parameters: optical thickness, single scattering albedo and asymmetry factor.

3.1.1 Optical thickness

Practically, this is the parameter of maximum influence on cloud reflectance and transmittance. It depends upon the drop size distribution, $n(r,z)$ through

$$\delta_\nu = \int_{Z_b}^{Z_t}\int_0^\infty n(r,z)\pi r^2 Q_{ext}(x,m)dr dz \tag{18}$$

where Z_b and Z_t are the altitude of the cloud base and cloud top respectively, r is the particle radius, $x = 2\pi r/\lambda$ is the Mie parameter and Q_{ext} the Mie efficiency factor which depends upon the refractive index $m = m' - im''$. Cloud particles are generally large compared to the wavelength($x \gg 1$). In these conditions it can be shown that Q_{ext} is close to 2 [Van de Hulst,1957]. Then, the optical thickness is directly proportional to the liquid water path W:

$$\delta_\nu \simeq \delta = 3W/2\rho r_e \tag{19}$$

where $W = \int_{Z_b}^{Z_t} w(z)dz$ with w the liquid water content, $r_e = \int_0^\infty n(r)r^3dr / \int_0^\infty n(r)r^2dr$ the effective radius of the size distribution and $\rho = 10^3 kg.m^{-3}$.

The liquid water content can reasonably be considered as a predictable quantity in climate models (see for example Sundqvist, 1984) but the drop size distributions (DSDs) are probably not predictable in the next future. The strong dependence of the optical thickness on the effective radius is thus a difficulty. However, observations show that liquid water contents and DSDs are correlated, larger w being associated with larger particles [Paltridge, 1974].

The problem is quite different according to whether one considers the fine variations of r_e within a particular cloud or one searchs for some empirical relationship which is assumed to apply statistically to any cloud system and is derived from a large set of observations in different

conditions. In the first case, assuming that the DSD follows a modified gamma distribution [Deirmendjian, 1969]

$$n(r) = ar^\alpha e^{-br}, \tag{21}$$

one can easily show that

$$r_e = k(w/\rho N)^{1/3} \tag{22}$$

where $N = \int_0^\infty n(r)dr$ is the total number of drops per unit volume.
The proportionality coefficient k only depends on α. It is typically of the order of 0.70 μm with extreme values of 0.62 and 1.02 μm. Inside a cloud such as a stratocumulus, N is roughly independent of the altitude (see for example Slingo et al, 1982 b; Nicholls and Leighton, 1986). In these conditions, r_e is clearly proportional to $w^{1/3}$; this is the basis of the modelling used in section 3.2 for the discussion of the cloud absorption.

In this section, on the contrary, we are interested in the bulk properties of clouds and what we need is a statistical relationship between r_e and w or W in order to be able to derive the optical thickness from the specification of the liquid water content. Even though N is roughly independent of the altitude within a given cloud, it is highly variable from one cloud to another or even within the same cloud, from one region to another; this makes relation (21) useless in the present context. However, even though the diversity of cloud characteristics makes relatively obscure the idea of "standard clouds", one can agree that the eight clouds that Stephens [1978a, 1979] considered are representative. For these clouds there is clearly an increase of r_e with w which can, very roughly, be parameterized as

$$r_e = 11w + 4, \tag{23}$$

where r_e is in μm and w in gm^{-3}.

The use of the empirical relation (22) together with approximation (19) defines the optical thickness.

..1 Asymmetry factor

With the noticeable exception of the 2.7μm absorption band, the asymmetry factor of liquid water clouds shows little variation with either wavelength or DSD [Stephens, 1979]. In addition, as noted by Slingo and Schrecker [1982], cloud radiative properties depend only weakly upon the asymmetry factor. Except for particular cases, an average value of $g \simeq 0.85$ gives satisfactory results for low level clouds.

..2 Single scattering albedo

The single scattering albedo ω_ν is the probability that a photon is scattered when interacting with a particle. The co-albedo $1 - \omega_\nu$ is therefore the probability of absorption. Keeping in mind the role of the solar heating in the generation of turbulent kinetic energy in low-level clouds, ω_ν is clearly a key parameter. The absorption coefficient of liquid water is very small in the visible part of the spectrum, but increases in the near IR and since about 30% of the incoming solar

irradiance correspond to the range 1 μm to 4 μm, the cloud drop absorption is quite important. The shortwave cloud absorption, however, is not only due to droplets absorption; the molecular absorption, mainly by water vapor, is modified by the multiple scattering. This problem is considered in more details in section 2.2.

In order to take the droplet absorption into account in radiation models at low spectral resolution, one has to define some equivalent single scattering albedo ω_e. Empirically, we found that ω_e is not very sensitive to the DSD, as long as stratocumulus are considered, but increases with the optical thickness (this is directly related to the saturation of the liquid water absorption bands). The following approximation is based on calculations performed in the case of a mid latitude summer atmosphere [Mc Clatchey et al, 1971] and accounts for water vapor as well as liquid water absorption.

$$1 - \omega_e(\delta) = 10^{-3}\left(0.9 + 2.75(cos\theta_0 + 1)\, e^{-0.09\delta}\right). \qquad (23)$$

where θ_0 is the solar zenith angle. Applying this approximation to the calculations of absorptances gives accuracies better than 1%.

3.1.4 Comparison with observations

Since approximate methods of solving the radiative transfer equation in scattering medium are accurate enough for calculating irradiances and still very cheap in terms of computer time, the most appropriate way to characterize the bulk optical properties of low-level clouds is to derive the cloud optical thickness from (19) and (22) and the single scattering albedo from (23), the asymmetry factor being fixed to $g = 0.85$. From our point of view, this method is the most appropriate in climate modelling as it clearly identifies the range of validity of the different approximations to be used, as well as the place of the empiricism in the parameterization, that is the relationship between r_e and the liquid water content. With the availability of new observations this relationship should differentiate according to the type of clouds under consideration or according to the mechanism responsible of their generation.

To test this method we tried to summarize (Table 3) the results of observations performed in many locations and available in the literature. When possible the cloud reflectances, absorptances and transmittances have been calculated using the Delta-Eddington approximation [Joseph et al, 1976], one of the most commonly used approximate method for solving the radiative transfer equation, together with the above parameterization of δ, ω_e and g. However, in many occasions, it was not possible to get all the needed informations (that is, liquid water path, cloud thickness, solar zenith angle, surface reflectivity).
According to these observations the liquid water path (W) of stratus and stratocumulus clouds ranges roughly between 10 and 200 gm^{-2}, the largest value (450 gm^{-2}) reported in Table 3 corresponding to a mixture of stratocumulus, altostratus and nimbostratus. Consequently, the shortwave optical thicknesses according to (19) and (21) vary from 2 to 50. Trying to relate *outside* observations of cloud reflectances and transmittances to *inside* measurements of cloud microphysics is generally a rather difficult exercise as clouds are, only exceptionally, homogeneous and stable enough. Despite of these difficulties, cloud reflectances and transmittances calculated from the parameterized relationships agree fairly well with observations (see Figure 5a). At least, the agreement is quite comparable to what other authors obtained from more

complete observations and more detailed calculations (compare Figures 5a and 5b). This shows that the proposed parameterization of optical thickness, single scattering albedo and asymmetry factor is satisfactory.

3.2 Solar absorption

As outlined previously, the absorption of solar radiation in clouds is very important in many aspects: (1) It reduces the quantity of energy reflected back to space or incident at the surface. Among other consequences, uncertainties in cloud absorption may lead to very substantial errors in the derivation of surface shortwave radiation from space. It is often assumed that the globally averaged cloud absorption is close to 5/absorption would increase be roughly 8 Wm^{-2} if we assume a 50% cloud cover; this is nearly twice as large as the change of the net longwave irradiance at the tropopause which would result from a doubling of the atmospheric CO_2. (2) The solar absorption results in quite a significant heating of the cloud layer. This may have important consequences on the dynamics of the atmosphere as well as on the life of the cloud [Bougeault, 1985; Byrd and Cox, 1984].

The cloud absorption is particularly difficult to measure so that it is not surprising to see a large dispersion in the reported observations (see Figure 6). The problem is that many authors observed much larger absorptions than predictable. Reynolds et al [1975] reported absorptances in the range 12 to 36% for stratocumulus clouds and 35 to 40% for cumulus, Drummond and Hickey [1971] observed absorptances of 25% in cumulus, and Neiburger [1949] absorptances of 30% in stratiform clouds. As shown by Stephens et al [1978], these observations strongly desagree with the theory, and would correspond to some "anomalous absorption". In this section, we consider the possible physical reasons explaining these puzzling observations and try to delineate more clearly the problem.

The simulation

From a purely theoretical point of view, the true absorption of solar radiation in clouds can be attributed to a combination of absorptions by atmospheric gases, liquid or solid water and aerosols. In this section we limit the review to liquid water clouds. To illustrate the purpose, simulations were made for a stratocumulus observed West of Brittany in October 1982 during the NEPHOS experiment [Fouquart, 1985]. The cloud top height was about at 550 m and the cloud base varied from 550 m (no cloud) to 100 m. According to Betts [1973] and Deardorff [1976], the liquid water potential temperature (or equivalently the moist static energy $h = CpT + gz + Lq$), and the total water specific humidity are independent of height inside the cloud. Hence, the liquid water content w increases linearly with height (Figure 7a). The total number of drops was roughly independent of height ($N \simeq 350\ cm^{-3}$); the corresponding variation of r_e calculated from (21) is reported on Figure 7b. The atmospheric profile, based on radio-soundings and aircraft observations, was roughly similar to the U.S. Standard Atmosphere, 1976. Irradiances were calculated using a narrow-band model (208 spectral intervals between 0.20μm and 4μm) which has been tested in the Intercomparison of Radiation Codes in Climate Models (ICRCCM)[Ellingson and Fouquart, 1989] and found to be accurate within a few Wm^{-2} when compared with line-by-line models and with the other high spectral resolution codes.

Molecular absorption

In the shortwave, the molecular absorption, mostly attributable to water vapor, may be enhanced because of the increase of the photon optical paths due to multiple scattering. This enhancement depends on the radiation field itself, particularly on the spectral characteristics of the radiation incoming at cloud top, in relation with the saturation of the water vapor absorption bands. Therefore, the efficiency of multiple scattering at increasing molecular absorption is maximum when the atmosphere above is dry, but it obviously depends also on the water vapor amount within the cloud layer. During the NEPHOS experiment, the total water vapour amount was 1.5 $g.cm^{-2}$, among which 1.0 $g.cm^{-2}$ above the cloud top. Figures 8 show the variation of the absorptance with the cloud thickness or, equivalently, the liquid water path W. Three cases are considered: the clear air absorptance of the layer in which the cloud is located and the cloud layer absorptance without and with the cloud drop absorption. The difference between the first two curves illustrates the enhancement due to multiple scattering. In the present case, for moderate water vapor amounts, the molecular absorption culminates to 2% for a layer 450 m thick; Wiscombe et al [1984] found much larger molecular absorptions when they considered cloud layers 2 to 4 km thick in a tropical atmosphere. Stephens [1978a, 1978b] performed similar calculations; he concluded that for short to moderate water vapor paths, multiple scattering enhanced the molecular absorption from roughly 1% for thin stratus clouds to 8% for thick and moist clouds but reduces it for longer paths. According to the present simulations, there are another cases for which the presence of cloud particles results in a decrease of the absorption within the layer (compare Figure 8a for $\theta_0 = 66°$ with Figure 8b for $\theta_0 = 37°$). This is dependent upon the sun zenith angle and is due to the reflection of radiation out of the layer. For low solar elevations, scattering privileges the reflection so that the radiation beam does not penetrate into the layer enough to be absorbed. For high elevations, the reflection is weaker and concerns photons which have travelled deeper in the layer.

Cloud drop absorption

Figures 8 show a strong increase of the absorptance when the cloud drop absorption is added. However, at very low solar elevations, a large number of photons are reflected without entering enough into the cloud layer to be absorbed so that the absorption can still be reduced compared to the clear air case [Wiscombe et al, 1984].

Practically, in clouds, liquid water content and drop size distribution are related; in the present simulation, r_e and w are linked by the relation (21) and W is proportional to the square of the cloud geometrical thickness ΔZ. The increase of the absorption with ΔZ is thus amplified: if the DSD were kept constant to its value for $\Delta Z = 50\ m$, the absorption would culminate to roughly 5% instead of 7%.

The dependence of the absorption on r_e is rather complex. An increase of r_e at constant optical thickness δ results in an enhanced absorption, since the single scattering albedo ω decreases [Irvine and Pollack, 1968; Twomey and Bohren, 1980], whereas if W is constant there are two opposite effects to consider: ω decreases but δ decreases too (see Equation (19)). For very thick clouds the first effect predominates whereas for thin clouds, Wiscombe and Welch [1986] and Ackerman and Stephens [1987] have shown that the decrease of δ, whose impact is the largest, tends to reduce the absorption. Table 4 shows the results of the present simulation, in agreement with these conclusions. Note that the reduction is much smaller at low solar elevations, a cloud being optically thick much more rapidly in this case.

The shortwave cloud absorptances, *Abs*, in Table 4 are much smaller than many of the observed values reported in Table 3. However, since for thick clouds *Abs* increases with r_e, one can question if the presence of very large drops could explain the "solar absorption paradox". Wiscombe et al [1984] considered different DSDs with r_e varying from 12 to 55 μm; they concluded to only a moderate increase of *Abs*. Hegg [1986] noticed that effective radius of several hundreds of μm were frequently reported even in non precipitating clouds. Wiscombe and Welch[1986] thus considered distributions with effective radius up to $r_e = 216\ \mu m$ and obtained absorption enhancements up to 8% compared to the standard cases without very large drops.

This explanation, however is unsufficient at least for three reasons:

1. In the literature, there are very few reports of simultaneous observations of irradiances and size distributions including the classes of very large drops. Nicholls [1984] and Stephens and Platt [1987] observed a significant proportion of large drops ($r \geq 50\mu m$) in low level clouds. We also observed such large drops during NEPHOS. However their proportion is much too small to arrive to the effective radius reported by Hegg.
2. According to Nicholls [1984], the relative concentration of large drops decreases with altitude. According to Newiger and Bähnke [1981], if the very large drops are located near the cloud base, their impact on the cloud absorptivity is minimized , mostly due to the fact that most of the reflected photons have not penetrated deep enough in the cloud to encounter these large drops.
3. To obtain their result Wiscombe and Welch had to consider very thick clouds. The 8% enhancement of *Abs* corresponded to $W \simeq 5000\ gm^{-2}$. For stratus and stratocumulus clouds W is typically of the order of 10 to 200 gm^{-2}.

Aerosol absorption

Simultaneous observations of aerosol concentration and optical properties, cloud microphysical characteristics and radiation are exceedingly rare and FIRE represents the first opportunity to get such a comprehensive data set. The condensation nuclei are known as having the potential of increasing cloud reflectivity at constant W by decreasing the drop size [Twomey, 1977]. However, in this section, we just consider the role of unactivated aerosols in cloud absorption, by keeping constant the cloud characteristics.

The influence of unactivated aerosols depend upon their concentration and nature: sea-spray aerosols are practically non absorbing whereas soot particles are extremely absorbant. These two characteristics are extremely variable in space and time and generally speaking, very badly known.

In the present simulation, we made the simplifying hypothesis of totally hydrophobic aerosols and we kept the aerosol optical thickness δ_a constant for three types of aerosols: maritime, continental and urban-industrial [WCP 112, 1986]. We chose $\delta_a = 0.4$ between the surface

and the cloud top height, i.e. an extinction coefficient of 0.73 km^{-1}, a large but not unrealistic value.

Figures 9 show for both clear and cloudy conditions the variation with ΔZ of the additional absorption due to the interstitial aerosols. Not surprisingly, the maritime aerosols give a very small additional absorption (0.1% per 100 m) to be compared to 1% for continental and 2 to 4% for industrial aerosols. The enhanced layer reflectivity in cloudy conditions explains that the aerosol effect is smaller for cloudy than for clear conditions for the larger solar zenith angle; on the contrary, for $\theta_0 = 37°$, the enhancement of the path length by the multiple scattering predominates, resulting in the opposite effect but less and less as the cloud becomes thicker.

In the present hypothesis of hydrophobic aerosols, the additional absorption due to aerosols is thus about two times smaller in a cloud than in clear atmosphere for $\theta_0 = 66°$ and of the same order for $\theta_0 = 37°$. Aerosols are generally not completely hydrophobic. A detailed analysis of the properties of mixtures of soot and liquid water has been performed by Chylek et al [1984]. They showed that in case of carbon randomly distributed throughout the volume of a droplet, the specific absorption of a water-graphitic carbon internal mixture was more than twice as large as for an external mixture. Consequently, there should be some amplification of aerosol absorption in cloudy conditions.

With respect to the solar absorption paradox, Figures 9 clearly show that under polluted conditions, a stratocumulus cloud could theoretically experience very strong absorptions (roughly 21% and 16% for $\theta_0 = 37°$ and 66° respectively, for a cloud 450 m thick). However, most, if not all of the observations have been performed in regions which are not particularly polluted. In particular, above the oceans where most of the data reported in Table 3 have been collected, the additional aerosol absorption should be small, at least if the aerosols to be considered are of maritime origin. In any case, if the contribution of aerosols is significant, Figures 9 show that their absorption should also be significant in the clear atmosphere surrounding the cloud layer; it should thus be measurable using the same technique as for cloud layers, as Fouquart et al [1988] did for desert aerosols.

The effect of cloud inhomogeneities

At this stage, one can question whether the anomalous absorption exists really. An obvious cause of possible overestimation of cloud absorption is that, for finite clouds, a part of the incident solar irradiance emerges from the cloud sides and may be missed in the final balance. In this section we consider only the case of clouds whose horizontal extension is sufficient to minimize this problem.

The cloud absorption is derived from upward and downward irradiance measurements performed at cloud top and cloud base from airborne pyranometers. The result is thus highly unaccurate mainly because it assumes (i) that the cloud layer is horizontally homogeneous and (ii) that the cloud remains stable during the measurement process. In addition the absorption results from two successive differences between large quantities and is obviously highly sensitive to the uncertainties which affect each component; in particular, the non uniform cosine response of the pyranometer and the pitch and roll of the aircraft is responsible of large uncertainties in the measurements of the incoming irradiance [Foot et al, 1986].

Generally, cloud absorptances are determined from measurements made by a single aircraft. In this case, because of the large spatial and temporal cloud variability, the irradiances measured at the base of the cloud layer do not necessarily correspond to those measured at cloud top. Figure 10 depicts a situation that we observed during NEPHOS. A part of the flight leg was done above a layer whose optical thickness was $\delta \simeq 6$ according to the measured reflectance, the second part over a visibly thicker layer ($\delta \simeq 20$). Table 5 shows the calculated apparent absorptance according to the flight legs used. Whereas the true absorptance varies from 2 to 6%, the apparent one may be quite large (nearly 30% in the worst case) or even negative. Figure 11 illustrates this effect: it presents a 10 sec. smoothed record of the time variation of upward, downward and net irradiances during a descent in the stratocumulus of Figure 10; this descent corresponds to a horizontal length of approximately 15 km. Note the apparent increase of the net shortwave irradiance during the descent (30 Wm^{-2}) as a result of the reduction of the cloud optical thickness. Such non physical results are frequent; in the case of a cloud thinning, they are easily detectable; in the reverse case, it is much more difficult to distinguish between enhanced absorption and variations of the cloud structure.

A rather more reliable method consists in deriving the shortwave absorptance from multispectral measurements. Ackerman and Cox [1982] used the usual ($0.3 - 2.8\mu m$) pyranometers plus a pair of red domed ones ($0.7 - 2.8\mu m$). Assuming that the actual visible ($0.3 - 0.7\mu m$) absorptance is negligible, they can correct the measured absorptance from the effect of cloud structure variations by subtracting the apparent visible absorptance. We applied this technique to our simulation. The corrected absorptances reported on table III are much closer to the true ones. However, a fundamental hypothesis is that the cloud absorption occurs totally in the near IR ($\lambda > 0.70\mu m$); thus aerosols absorption occurring in the visible window cannot be detected. If, for example, we consider a cloud identical to that of the thickest part of the stratocumulus of Figure 10, polluted by industrial aerosols of optical thickness $\delta_a = 0.4$ as in section 2.2, the "corrected" absorptance would be $\simeq 2\%$ whereas the actual one would be 13 and 16% for $\theta_0 = 67°$ and 37° respectively. Clearly, the bispectral method is very strongly biased and does not provide, by itself, a definite answer on the effectiveness of an observed anomalous absorption. However, if utilized in conjunction with absorption measurements in the clear air nearby the cloud, it does represent a significant improvement.

A more sophisticated technique makes use of detailed spectral measurements of the radiances reflected or transmitted by the cloud layer. Compared to the bispectral irradiance technique, this method has two big advantages: (i) the spectral resolution of the observations generally allows to distinguish in the near infrared between water vapor absorption bands and continua and (ii) the radiances are much more sensitive to small scale fluctuations of the cloud characteristics which can thus be identified and accounted for. Curran et al [1981], Stephens and Scott [1985] and Foot [1988] described the characteristics and performances of specially designed radiometers; Stephens and Platt [1987] and Foot [1988] presented the results of airborne measurements of the spectral reflectance, whereas Rozenberg et al [1974] reported on similar observations from a Kosmos satellite. They all reported on spectral behaviours which differed significantly from those of plane-parallel pure liquid water clouds. Foot showed that cloud top small scale ($\simeq 25m$) structures could be the cause of some of these anomalies but they had almost no impact on the cloud absorption. Figure 12 shows the spectral reflectivities of (i) the thickest part of the stratocumulus of Figure 10 ($\delta = 20$, $r_e = 7\mu m$, $\Delta Z = 300m$ and $\delta_a = 0$, i.e. no aerosols), (ii) the same cloud polluted by industrial aerosols ($\delta_a = 0.4$) and (iii) a non polluted cloud similar to that of case (i) but with the Stephens [1978] cumulonimbus DSD ($r_e = 31\mu m$).

To get roughly similar values of the spectrally integrated reflectance for all three cases, the liquid water reference optical thickness (δ, see Equation (19) has been kept constant. It can be seen that

1. the influence of the DSD at constant δ is very small in the visible but becomes very large in the near infrared ($\Delta R \sim 1\%$ in the visible, 15% near $1.65\mu m$ and 20% near $2.3\mu m$). Complete calculations showed moderate difference in total absorptance: 8% for the larger drops compared to 5% for the standard case. This relatively small impact is due to the spectral distribution of the incident solar irradiance which privileges the visible part.

2. the impact of aerosols is much more uniform over the whole solar spectra. This is directly linked to the spectral variation of the aerosol complex index of refraction. However, as noted for soot particles by Chylek et al [1984], the aerosol effect decreases with the wavelength. For the particular cases reported on Figure 12, δ is constant , the spectrally integrated reflectance is thus a bit smaller with aerosols ($R = 69\%$ instead of 73%). Indeed, δ can be adjusted to get exactly the same total reflectance; in this case the spectral differences remain smaller than $\pm 2\%$; however, the total cloud absorptance increases much more substantially, from 5% without aerosols to 12% for the polluted case.

A non ambiguous answer as for the reality of the anomalous absorption requires very significant instrumental improvements. The accuracy of the usual pyranometers meets only marginally those required for the normal absorption in stratocumulus. Preferably, cloud absorptances should be derived from quasi instantaneous observations of spectral reflectances which intrinsically account for possible variations of the upper boundary conditions and, when saturated for thick clouds, are strongly dependent upon the single scattering albedo. Another powerfull approach consists in measuring the angular distribution of the scattered radiation deep inside the cloud, in the region of the diffusion regime [King, 1981; King et al, 1986]. Measurements of aerosol concentration and optical properties are also needed and should systematically accompany the usual microphysical measurements; in addition direct observations of the clear air absorption in the immediate surrounding of the cloud layer should be performed whenever possible.

4 The influence of clouds on the longwave radiation

The usual approximation, in the longwave, is to neglect scattering and consider cloud droplets as purely absorbing particles. This is mainly justified because of the very strong molecular absorption out of the IR window ($8\ 14\mu m$) which limits the impact of the liquid water on the radiation field to that spectral range where the scattering efficiency of particles with dimensions typical of non precipitating clouds is much smaller than in the visible. Another important but often neglected reason lies in the fact that the distribution of the sources of radiation is obviously much more isotropic than in the shortwave, thus reducing the role of scattering. For Cirrus clouds, the scattering may play a more important role due to both the larger difference between the incoming radiation at cloud top and cloud base and the smaller asymmetry factor of crystals leading to larger reflectivities [Stephens, 1979].

Neglecting the scattering effects, the transmission through the cloud layer for a viewing zenith angle $\theta \quad cos^{-1}\mu$ is

$$t(\mu) \; - \exp\left(- \frac{1}{\mu} \int_{Z_b}^{Z_t} K_{abs}(\lambda, z) dz \right) \sim \exp(\quad kW/\mu) \tag{24}$$

where $K_{abs}(\lambda, z)$ is the absorption coefficient, k a mass absorption coefficient theoretically frequency dependent and W is still the integrated liquid water path.

The vertical emittance is thus

$$\epsilon_\lambda = 1 - t_\lambda(\mu = 1) = 1 - \quad exp(\quad kW). \tag{25}$$

To calculate the longwave irradiances, a diffuse emittance ϵ^d is needed; one generally uses the diffusivity factor $R = 1.66$ [Elsasser, 1942], so that

$$\epsilon_d \simeq 1 - exp(- RkW). \tag{26}$$

Platt [1976], Stephens et al [1978], Bonnel et al [1983], Slingo et al [1982a] determined experimentally a mass absorption coefficient averaged on the IR window. According to Stephens et al [1978], $Rk \simeq 0.158(gm^{-2})^{-1}$. Among other things, Figure 13 allows to test the validity of the above parameterization. Figures 13a show the profile of the liquid water content observed during an ascent at low vertical speed ($100\ ft/min$) during NEPHOS ; two idealized longwave profiles were considered : one including the cloud top rolls, the other one excluding them. In their lower part the idealized profiles were based on the hypothesis of a constant total water mixing ratio in the mixed layer. Figure 13b shows the longwave upward and downward irradiances, observed (solid lines) and calculated for both idealized longwave profiles. The influence of the rapid variation of the emissivity (from 0 to 1) can easily be seen in the upper part of the cloud. The dashed lines correspond to the results of Stephens' parameterization, whereas the stars correspond to calculations using a scattering model developed by Morcrette [1978]. The accuracy of approximation (26) is quite spectacular.

Cloud top longwave cooling

The cloud top radiative cooling is a factor of extreme importance in cloud dynamics, particularly for clouds in the lower layer of the atmosphere (the boundary layer) since it drives the entrainment of dry air from above and is a major source of turbulent kinetic energy within the boundary layer [Deardorff, 1976; Schubert et al, 1979; Fravalo et al, 1981]. The main problem concerns the area-averaged thickness of the radiatively cooled layer [Randall et al, 1984]. Figure 13a shows that the vertical extension and the liquid water content of the well organized rolls observed during this particular flight were quite large (roughly $60 - 70m$ and $w \simeq 0.5gm^{-3}$) ; according to horizontal legs performed at cloud top, through the rolls, the wavelength of the rolls was about $600m$.

Figure 13c shows 90% of the cloud top cooling occurs within a layer 80 m thick inside the cloudy air, either below the top or the base of the rolls, in good agreement with previous observations [Slingo et al, 1982 a, b; Bonnel et al, 1983]. Because of their smaller liquid water

path, the regions corresponding to the troughs do not evidence a longwave heating at cloud base; in addition the radiative cooling of the regions of the troughs also interests the regions of dry air which are cooled by the surrounding turrets. These features may have a significant impact on the dynamics of the cloud and deserve more attention.

5 The effect on the radiation field of horizontal inhomogeneities

Given the delicate balance between clouds and climate, small systematic errors in the radiative behavior of clouds may be significant. Since cloudiness is known to exhibit heterogeneities at various spatial scales, the most obvious limitation of the current estimates of the effect of clouds on radiation probably lies in the plane parallel hypothesis. Much effort has therefore been expended in recent years in studies of the radiative properties of broken clouds.

Relaxing the plane-parallel idealization raises serious problems both with regard to realistic descriptions of broken cloud fields and calculations of their radiative properties, particularly at solar wavelengths. Experimental investigations of the statistical morphology of real cloud fields are under way. From detailed analysis of high resolution satellite imagery it is possible to retrieve the number density of cloud cells as a function of their mean dimension [Welch and Wielicki, 1986; Wielicki and Welch, 1986; Parker et al, 1986]. However, a conceptual framework for describing statistically the variability of the shapes, sizes and spatial organization of clouds is still lacking and will need considerable efforts.
On the other hand, solutions of the radiative transfer problem in media other than the usual plane-parallel one are difficult, and accurate and fast techniques do not exist yet. Exact methods [Preisendorfer and Stephens, 1984] or analytical treatments based on the Eddington approximation [Davies, 1978; Gube et al, 1980] have been developed. These solutions may provide valuable benchmarks and they are efficient at investigating the influence of some cloud parameters, but they have only been developped for isolated clouds with simple cuboid geometries, and their extension to other geometries and cloud arrays is by no means immediate. Therefore, most studies of radiative transfer in finite clouds have been based on numerical simulations using the Monte Carlo technique, which is particularly suited to this problem because of its ease to modelling any geometry. However, while potentially very versatile for isolated clouds, the Monte Carlo technique is still limited when addressing the problem of cloud field assemblies. As a consequence, given the limiting factor of the computation time, Monte Carlo simulations must practically restrict to regular arrays of clouds in order that symmetry considerations allow that the photon trajectory could be tracked easily from one single reference cloud.

Finally, the present state of the art in finite cloud modelling consists in no more than regular arrays of uniform, simply shaped clouds (cubic, hemispheric, cylindric ...), just arranged in infinite chess board patterns. These are the most sophisticated models which are numerically tractable in the shortwave domain. On the other hand, whatever crude these models are compared with the complexity of real cloudiness, they seem flexible enough to provide significant insight about the specific radiative characteristics of broken cloud fields.

As previously, we distinguish in this section between the longwave and the shortwave problems. In both ranges, the main objective is to evaluate the energetic impact of radiation from

the point of view of general circulation or climate studies. Accordingly, irradiances are meant as average values over rather large areas, with typical dimensions of several kilometers. Clearly, in order that the previously described modelling make sense, the parameters characterizing the kind of brokenness which the cloudiness exhibits are assumed to be invariant over the area. Thus, given the actual cloud cover A_C of the area, we mainly aim at retrieving the effective or equivalent plane-parallel cloud cover, A_e, defined as that fraction of a plane-parallel cloud which would provide the same radiation budget than the finite cloud field. Whatever the difficulty for evaluating A_e from detailed specific calculations, the possibility to keep plane-parallel parameterizations usable is a sufficient justification for this approach. As a second goal, we address the question of the bidirectional reflectance of heterogeneous cloud covers. While somewhat secondary from the energetic point of view, this question deserves attention, particularly in the shortwave range, on account of its implications for observational purposes [Davies, 1984].

5.1 Broken cloudiness and longwave radiation

5.1.1 The direct problem: effects of brokenness on irradiances

The influence of broken cloudiness on the transfer of infrared radiation through the atmosphere has been addressed by Ellingson [1982] and Harshvardhan and Weinman [1982]. At infrared wavelengths, the scattering of radiation is less important than geometrical effects [Harshvardhan and Weinman, 1982; O'Brien, 1986]. Accordingly, the clouds may be considered as black bodies, which considerably reduces the mathematical complexity of the problem. In these conditions, the plane-parallel approximation consists in neglecting the horizontal dimension of the clouds under consideration and in considering them as flat. The resulting longwave irradiances are just weighted averages of the irradiances calculated for completely clear and overcast conditions, with the actual cloud fraction A_C as the weighting factor for the cloud cover term.

Actually, since the clouds sides also interact with the radiation field, for any direction other than normal the effective cloud cover is larger than A_C. Therefore, shaped clouds result in more downward irradiance at the surface and, generally, less irradiance escaping the atmosphere than predicted by their plane parallel counterparts. This effect may be quite noticable; as shown by Ellingson [1982], planiform calculations may lead to errors as large as 10 to 20% in the estimated heating or cooling rates of the troposphere.

The elaboration of simple formulae to provide the effective plane-parallel cloud cover A_e, although mainly a geometrical problem when neglecting scattering effects, remains complex. The influence of brokenness depends on the cloud sizes and shapes, as well as some external parameters such as the atmospheric temperature and water vapor profiles.

The problem was addressed by Ellingson [1982], from the point of view of irradiance and heating rate evaluations, and by Harshvardhan and Weinman [1982], who, more particularly, paid attention to the radiance and irradiance escaping the atmosphere. Both studies showed the major influence on A_e of the cloud aspect ratio, a, i.e. the ratio of the mean cloud vertical dimension to their mean horizontal dimension. By comparison, the influence of the atmosphere

temperature profile, as studied by Ellingson, is much lesser. Moreover it must be stressed that, although Ellingson considered cylindrical clouds distributed according to a Poisson distribution whereas Harshvardhan and Weinman considered regular arrays of cubic clouds, the derived relationships $A_e = f(A_C, a)$, are very similar in both cases; their typical form is illustrated in Figure 14.

These results therefore indicate that the fractional cloud cover and the cloud aspect ratio are the main parameters for characterizing the cloud morphology; particular cloud shapes or spatial organization appear to be of secondary importance. Observations indicate that generally $a > 1$ [Planck, 1969], but the finiteness effect strongly varies for a ranging from 0.5 to 2. As predictable, the effective plane parallel cloud cover is always larger than the real one, and, the larger a, the larger the difference. As A_e obviously is identical to A_C for small cloudiness and full cloud covers, the brokenness effect is maximum for A_C ranging from about 0.40 to 0.70.

Therefore, accounting for brokenness in estimates of the infrared radiative effect of cloudiness seems quite tractable. Some refinements are probably necessary in order to take into account the effect of cloud shape, size distribution, cloud overlap or scattering. Such effects, however, consist very probably in no more than correcting terms.

5.1.2 The indirect problem: directional effects of brokenness

Because of the cloud sides influence on the infrared radiance, broken cloudiness exhibits directional effects which differ significantly from those of planiform clouds. This was studied by Naber and Weinman [1984], by using simultaneous observations of broken cloud fields from the GOES East and GOES West satellites. They found that depending on cloud cover and aspect ratio, the cloud side effect may amount to differences in apparent brightness temperature as large as $8K$ according to the viewing direction. By adjusting the aspect ratio in their model of broken clouds, Naber and Weinman [1984] obtained convincing fits of the observations. Duvel and Kandel [1984] considered the influence of unresolved broken clouds on satellite estimates of outgoing longwave irradiances. More specifically, they simulated a sort of "cloud street" organization through a regular array of infinitely long parallel bands of clouds of rectangular cross sections. They concluded to possible biases as large as $30 W m^{-2}$, depending on the viewing conditions. This confirms that, as noted by Harshvardan [1982], satellite measurements of the outgoing longwave radiation cannot be used to deduce the climatic impact of clouds without informations on the subgrid scale cloud organization.

5.2 Broken cloudiness and shortwave radiation

For shortwave radiation, broken cloudiness essentially raises the problem of scattering by heterogeneous media. Although scattering and absorption of solar radiation are linked, the energetic impact of absorption is significantly smaller than the albedo effect. Moreover, as shown by Davies et al [1984], estimates of the absorption from plane-parallel parameterizations result in relatively small errors in the case of broken clouds. Therefore, for the sake of clarity, we restrict the present review to the albedo problem in the somewhat academic case of non absorbing clouds.

5.2.1 The direct problem: effects of brokenness on irradiances

This problem was first addressed for isolated cubic clouds by Mc Kee and Cox [1974] on the base of Monte Carlo simulations; then Davies [1978] used an Eddington approximation. For this simple case, these authors clearly showed the essential features linked to the influence of the sides of finite isolated clouds. The problem of including the cloud cloud interactions and the effects of mutual shadowing was then approached, with increasing accuracy and completeness, particularly by Aida [1976], Claussen [1982], Welch and Wielicki [1984] and Kite [1987]. The main results of these studies may be sum up in three characteristic behaviors that broken cloudiness exhibits as a result of geometrical effects:

1. First consider the intrinsic reflectance of a finite isolated cloud (Figure 15a), R_c, defined as the ratio of the total upward scattered irradiance on the total irradiance received from the directional sunbeam. As a result of the escape of photons through the sides of the finite cloud, regardless of the solar zenith angle θ_0, R_c is definitely lower than the reflectance R_p of a plane-parallel cloud with nearly the same optical thickness.

2. Then consider a horizontal area S which some cloud field is arranged on (Figure 15b). Let A_C still be the actual fractional cloud cover. To simplify, let us assume that the broken clouds are constituted of n spheres of radius r, such that $n\pi r^2 = ns = A_C S$. When the sun angle varies, the solar energy intercepted by the whole area is proportional to $S \cos\theta_0$. For the cloudy part A_C, it is proportional to $A_C S \cos\theta_0$ if A_C can be considered as made of plane parallel clouds. The broken cloud case is very different: the cross section is $A_C S$, whatever θ_0. Therefore, neglecting the clear air reflectance, the reflectance of the total area is $R_{pf} = A_C R_p$ for a plane-parallel cloud field, and $R_{bf} = A_C R_c / \cos\theta_0$ for the broken cloud field. This gain in photons captured by the cloud sides eventually compensates the corresponding increase in photon escape.

3. Of course, this gain is only efficient if there is no significant mutual shadowing effects of the clouds. If we except the case of normal sun incidence, it is clear that beyond some critical cloud cover, the neighbouring clouds progressively obscure the sides of the finite cloud, thus reducing the expected gain by photon capture.

To crudely illustrate these effects, let us consider purely lambertian spheres, i.e. such that the radiance should be constant for any point of their surface, in any direction. In fact, this heuristic model mimics the radiances escaping from a uniform sphere whose optical thickness is about 15 [Cretel et al, 1988]. The reflectance R_p of a plane parallel cloud of that optical thickness varies between about 0.55 and 0.65 according to θ_0, and this is larger than R_c, which obviously is $R_c = 0.5$ for the lambertian cloud. Then considering as previously n isolated spheres arranged over some horizontal surface S, $R_{bf} = 0.5 A_C / \cos\theta_0$, to be compared with $R_{pf} = A_C R_p$ for the planiform cloud. The resulting effective plane-parallel cloud cover, i.e. $A_e = A_C / (2R_p \cos\theta_0)$, smaller than A_C for normal incidence, increases with θ_0 as a result of the gain in photon capture, and becomes larger than A_C for large enough solar zenith angles. Of course, the apparent area $S \cos\theta_0$ is completely filled with the $A_C \pi r^2$ cloud cross section provided that $\cos\theta_0 > A_C$. Therefore, beyond this limit, the shadowing effects intervene and lower the broken cloud efficiency at reflecting solar radiation.

These geometrical effects explain the characteristic behavior of the effective cloud cover A_ϵ as a function of A_c and θ_0, as illustrated in Figure 16. A more detailed analysis should account for the influence on A_ϵ of cloud shapes, cloud sizes, and cloud cloud interactions. In a first approximation, the cloud shape influence may be thought as accounted for by the way of the cloud aspect ratio. This is probably not sufficient. The problem was examined by Welch and Zdunkowski [1981] for isolated clouds. They showed that simple factors like mean optical thickness and total liquid water content were unable to scale the radiative behavior of differently shaped clouds. They argued that the importance of the cloud shape probably vanishes for large cloud covers; however, the analysis of Welch and Wielicki [1984] from detailed Monte Carlo simulations accounting for cloud cloud interactions and mutual shadowing shows persistent influence of the cloud shape and aspect ratio for large cloud cover. The problem of scaling parameter able to make equivalent different cloud cell shapes with regard to their reflectance therefore deserves more study.

Concerning the cloud cloud interactions, the problem was first addressed by Aida [1976], who pointed out that surrounding clouds did not alter the cloud reflectance for distances larger than about five times the cloud horizontal dimension. Obviously, interactions may be quite large for high cloud cover, but the question is about the resulting modification of the reflectance. According to the lambertian sphere model, how large the number of photons entering neibourghing clouds, they do not modify R_{bf} provided that the probabilities for finally escaping, upward or downward from the cloud layer are the same. Multiple interactions are important only for very large or very small cloud optical thicknesses, as a result of the failure of the nearly lambertian approximation. Here again, there is presently no available accurate modelling of this complex effect, and the method adopted so far consists to consider clouds as lambertian diffusors when calculating cloud-cloud interactions, although this may be in error as shown by Claussen [1982].

Given the cloud cover, the predicted differences in the solar irradiances reflected by broken and plane parallel clouds may amount to 40 to 60 Wm^{-2} as shown by Welch and Wielicki [1984]. Note that the authors take into account, at least in an approximate way, the contribution of the clear sky molecular scattering, which tends to decrease the difference between plane-parallel and broken cloud radiative impact. This is clearly significant compared, for example, to the about 10 Wm^{-2} accuracy required by the ERBE experiment [Barkstrom, 1984]. Moreover, as shown by Harshvardhan [1982], the longwave and shortwave effects by no means compensate, so that taking into account the brokenness parameter in studies of the cloud radiative impact is clearly useful. Despite the needed improvements just outlined, modellings of A_ϵ have been elaborated whose degree of sophistication varies from purely or partly diffusive scattering models [Harshvardhan and Weinman, 1982; Joseph and Kagan, 1988] to fits of detailed Monte Carlo simulations [Welch and Wielicki, 1985]. The interest of such parameterizations is no dubious, as they make possible simplified analysis of the energetic impact of cloud brokenness.

5.2.2 The indirect problem: directional effects of brokenness

Bidirectional reflectance effects are expected from broken cloudiness in the shortwave range also. According to the reciprocity principle, the characteristic influence of the sun zenith angle upon the reflected irradiance, described previously, should entail, as a counterpart, increasing reflectance of finite cloud fields for increasing zenith viewing angles. Estimates of the bidirectional

reflectance of finite cloud fields, as calculated by Davies [1984], effectively exhibit large discrepancy from lambertian reflectance for moderate cloud cover. Obviously, these effects should have large implications for satellite measurements of top atmosphere irradiances at regional scales. Observational evidence of this effect, however, is still lacking for the moment. The only reported detailed observations of the shortwave radiation field of broken clouds are by Coackley and Davies [1986], from the NOAA-7 AVHRR data; the authors did not observe the expected increase in the apparent cloud cover with satellite view angle.

6 Conclusion

With reference to observations and detailed theoretical work, this paper reviewed several aspects of the effect of clouds on radiation and considered, the problem of their parameterization in climate models. Because of the lack of experimental data for high clouds, the review was mostly focused on low-level clouds. In this paper, we considered that climate models will soon include the condensed water as a pronostic variable and we examined how parameterizations based on this quantity can realistically simulate the radiation field.

Irradiance calculations in cloudy atmospheres depend on a set of specific frequency dependent cloud parameters, the optical thickness δ_ν, the single scattering albedo ω_ν and the scattering phase function $P_\nu(\Theta)$. It was shown in section 2.1 and 3 that simple parameterizations of these parameters together with approximate methods of calculation allow realistic simulations of observed bulk properties of extended liquid water clouds. In this approach, the shortwave optical properties of cloud layers depend on three spectrally averaged parameters : (i) the optical thickness δ, (ii) an equivalent single scattering albedo ω_ϵ and (iii) the asymmetry factor g. The longwave optical properties may be described through a single spectrally averaged parameter, the cloud layer emissivity ϵ_d. These parameters are functions of the cloud geometrical thickness and the total amount of liquid water present in a column of the cloud.

Extended ice clouds certainly require different parameterizations. However, in climate models, their radiative properties should, very likely, still be expressed through the same set of parameters; the question of their relation with the integrated ice content remains open and needs additionnal in-situ observations such as those performed during FIRE and ICE. By comparison, the problem of low level clouds is much better known. However two major questions remain: (i) in the case of extended clouds, how adequate are the present parameterizations to simulate the cloud absorption and (ii) in the case of broken cloud fields, how should the effects of brokenness with the usual plane-parallel approximation be simulated.

The cloud layer absorption may be attributed to absorption by (i) molecules, chiefly water vapor molecules, (ii) cloud drops and (iii) aerosols. For extended low level clouds such as stratocumulus, theoretical models calculated absorption of the order of 10 -15% or less. However, much larger values (up to 30%) were reported from different observations. Except for very polluted conditions, such large values can be considered as "anomalous". One possible explaination is that this large absorption is an artefact resulting from the large spatial and temporal variability that clouds experience at all scales.

Bibliography

Ackerman, T. P., and M. B. Baker, Shortwave radiative effects of unactivated aerosol particles in clouds, *J. Appl. Meteor.*, *16*, 63–69, 1977.

Ackerman, S. A., and S. K. Cox, Aircraft observations of the shortwave fractional absorptance of non–homogeneous clouds, *J. Appl. Meteor.*, *20*, 1510–1515, 1982.

Ackerman, S. A., and S. K. Cox, Shortwave radiative parameterization of large atmospheric aerosols dust and water clouds, *J. Geophys. Res.*, *93*, 11063-11073, 1988.

Ackerman, S. A., and G. L. Stephens, The absorption of solar radiation by droplets: An application of anomalous diffraction theory, *J. Atmos. Sci.*, *44*, 1574–1588, 1987.

Aida, M., Scattering of solar radiation as a function of cloud dimensions and orientation, *J. Quant. Spectrosc. Radiat. Transfer*, *17*, 303–310, 1976.

Albrecht, B., and S. K. Cox, The large scale response of the tropical atmosphere to cloud modulated infrared heating, *J. Atmos. Sci.*, *32*, 16–24, 1975.

Barkstrom, B. R., The earth radiation budget experiment (ERBE), *Bull. Amer. Meteor. Soc.*, *65*, 1170–1185, 1984.

Betts, A. K., Non precipitating cumulus convection and its parametrization, *Quart. J. Roy. Meteor. Soc.*, *99*, 178–196, 1973.

Bonnel, B., Y. Fouquart, J.-C. Vanhoutte, C. Fravalo, and R. Rosset, Radiative properties of some African and Mid- Latitude Stratocumulus Clouds, *Beitr. Phys. Atmosph.*, *56*, 409–428, 1983.

Bougeault, P., The diurnal cycle of the marine stratocumulus layer: A higher- order model study, *J. Atmos. Sci.*, *42*, 2826–2843, 1985.

Buriez, J. C., B. Bonnel, Y. Fouquart, J. F. Geleyn, and J. J. Morcrette, Comparison of model–generated and satellite– derived cloud cover and radiation budget, *J. Geophys. Res.*, *93*, 3705–3719, 1988.

Byrd, G. P., and S. K. Cox, A Case study of radiative forcing upon a tropical cloud cluster system, *Mon. Wea. Rev.* , *112*, 173–187, 1984.

Cess, R. D., Climate change: an appraisal of atmospheric feedback mechanisms employing zonal climatology, *J. Atmos. Sci.*, *33*,1831–1843, 1976.

Charlock, T. P., and V. Ramanathan, The albedo field and cloud radiative forcing produced by a general circulation model with internally generated cloud optics, *J. Atmos. Sci.* , *42*, 1408–1429, 1985.

Chou, M. D., Surface radiation in the tropical pacific, *J. Climate Appl. Meteor.*, *24*, 83–92, 1985.

Chylek, P., V. Ramaswamy, and R. J. Cheng, Effect of graphitic carbon on the albedo of clouds, *J. Atmos. Sci.*, *41*, 3076–3084, 1984.

Claussen, M., On the radiative interaction in three- dimensional cloud fields, *Beitr. Phys. Atmosph.*, *55*, 158–169, 1982.

Coackley, J. A., Jr., and R. Davies, The effect of cloud sides on reflected solar radiation as deduced from satellite observations, *J. Atmos. Sci.*, *43*, 1025–1035, 1986.

Cretel, D., M. Herman, and D. Tanre, Fluxes and directionnal effects for broken clouds, *Proc. Int. Rad. Symp.*, 95-98, 1988.

Curran, R. J., H. L. Kyle, L. R. Blaine, J. Smith, and T. D. Clem, Multichannel scanning radiometer for remote sensing cloud physical parameters, *Rev. Sci. Instrum.*, *52*, 1546–1555, 1981.

Davies, R., The effect of finite geometry on the three- dimensional transfer of solar irradiance in clouds, *J. Atmos. Sci.*, *35*, 1712–1725, 1978.

Davies, R., Reflected solar radiances from broken cloud scenes and the interpretation of measurements, *J. Geophys. Res.*, *89*, 1259–1266, 1984.

Davies, R., W. L. Ridgway, and K. Kyung Eak, Spectral absorption of solar radiation in cloudy atmospheres: a $20cm^{-1}$ model, *J. Atmos. Sci.*, *41*, 2126–2137, 1984.

Deardorff, J. W., On the entrainment rate of a stratocumulus topped mixed layer, *Quart. J. Roy. Meteor. Soc.*, *102*, 563–582, 1976.

Deirmendjian, D., *Electromagnetic Scattering on Spherical Polydispersions*, 292 pp., American Elsevier Publ. Co., New-York, 1969.

Drummond, A. J., and J. R. Hickey, Large scale reflection and absorption of solar radiation by clouds as influencing earth radiation budgets. New aircraft measurements, *Proc. Int. Conf. Weather Modification*, 267–276, 1971.

Duvel, J. P., and R. S. Kandel, Anisotropy of longwave radiation emergent from a broken cloud field and its effect on satellite estimates of flux, *J. Climate Appl. Meteor.*, *23*, 1411–1420, 1984.

Ellingson, R. G., On the effects of cumulus dimensions on longwave irradiance and heating rate calculations, *J. Atmos. Sci.*, *39*, 886–896, 1982.

Ellingson, R.G., and Y. Fouquart, The intercomparison of radiation codes in climate models (IRCCM): an update, *Proc. Int. Rad. Symp.*, 236-237, 1988.

Ellis, J. S., Cloudiness, the planetary radiation budget and climate, Ph D. Thesis, 129 pp., Department of Atmospheric Sciences, Colorado State University, 1978.

Elsasser, W. M., Heat transfert by infrared radiation in the atmosphere, *Harvard meteorological Studies n° 6*, 43 pp., Harvard University Press, 1942.

Foot, J. S., P. Hignett, and C.G. Kilsby, Investigation into errors associated with upwards facing pyranometers fitted to the MRF Hercules, *MRF Internal Note 31*, Available from the National Meteorological Office Library, Bracknell, 1986.

Foot, J.S., Some observations of the optical properties of clouds. I. Stratocumulus, *Quart. J. Roy. Meteor. Soc.*, *114*, 129–144, 1988.

Fouquart, Y., Radiation in boundary layer clouds, Report of the JSC/CAS Workshop on Modelling of Cloud Topped Boundary Layer , Fort Collins - USA, 22–26 April, 1985.

Fouquart, Y., B. Bonnel, G. Brogniez, J. C. Buriez, L. Smith, J.J. Morcrette, and A. Cerf, Observations of Saharan aerosols: Results of ECLATS field experiment. Part 2: Broadband radiative characteristics of the aerosols and vertical radiative flux divergence, *J. Climate Appl. Meteor.*, *26*, 38–52, 1988.

Fravalo, C. ,Y. Fouquart, and R. Rosset, The sensitivity of a model of low stratiform clouds to radiation, *J. Atmos. Sci.*, *38*, 1049–1062, 1981.

Geleyn, J. F., A. Hense, and H. J. Preuss, A comparison of model generated radiation fields with satellite measurements, *Beitr. Phys. Atmosph.*, *55*, 253–286, 1982.

Gube, M., J. Schmetz, and E. Raschke, Solar radiative transfer in a cloud field, *Beitr. Phys. Atmosph.*, *1*, 24–34, 1980.

Hanson, H. P., and P. L. Gruber, Effect of marine stratocumulus clouds on the ocean-face heat budget, *J. Atmos. Sci.*, *39*, 897–908, 1982.

Harshvardhan, The effect of brokenness on cloud– climate sensitivity, *J. Atmos. Sci.*, *39*, 1853–1861, 1982.

Harshwardhan, and J.A. Weinman, Infrared radiative transfer through a regular array of cuboidal clouds, *J. Atmos. Sci.*, *39*, 431–439, 1982.

Harshvardhan, D.A. Randall, T.G. Corsetti, and D.A. Dazlich, 1989: Earth radiation budget and cloudiness simulations with a general circulation model. *J. Atm. Sci. 46*, 1922-1942.

Hartmann, D.L., V. Ramanathan, A. Berroir, and G.E. Hunt, Earth radiation budget data and climate research, *Rev. Geophys.*, *24*, 439–468, 1986.

Hartmann, D. L., and D. A. Short, On the use of earth radiation budget statistics to studies of clouds and climate, *J. Atmos. Sci.*, *37*, 1233–1250, 1980.

Heise, A., and E. Heise, A sensitivity study of cloud parameterizations in general circulation models, *Beitr. Phys. Atmosph.*, 57, 240-258, 1984.

Herman, G.F., Solar radiation in summertime artic stratus clouds, *J. Atmos. Sci.*, *34*, 1423–1432, 1977.

Herman, G.F., and J. A. Curry, Observational and theretical studies of solar radiation in Artic stratus clouds, *J. Climate Appl. Meteor.*, *23*, 5–25, 1984.

Hegg, D. A., Comments on "The effects of very large drops on cloud absorption. Part I: Parcel model", *J. Atmos. Sci.*, *43*, 399–400, 1986.

Houghton, J. T. (Ed.), *The global climate*, 233 pp., Cambridge University Press, Cambridge, UK, 1984.

Irvine, W. M., and J. B. Pollack, Infrared optical properties of water and ice spheres, *Icarus*, *8*, 324–360, 1968.

Joseph, J. H., W. J. Wiscombe, and J. A. Weinman, Solar flux transfer through turbide atmospheres evaluated by the delta–Eddington approximation, *J. Atmos. Sci.*, *33*, 2452–2459, 1976.

Joseph, J. H., and V. Kagan, The reflection of solar radiation from bar cloud arrays, *J. Geophys. Res.*, *93*, 2405-2416, 1988.

King, M. D., A method for determining the single scattering albedo of clouds through observation of the internal scattered radiation field, *J. Atmos. Sci.*, *38*, 2031–2044, 1981.

King, M. D., and Harshvardhan, Comparative accuracy of selected multiple scattering approximations, *J. Atmos. Sci.*, *43*, 784–801, 1986.

King, M. D., M. G. Stange, P. Leone, and L. R. Blaine, Multiwavelength scanning radiometer for airborne measurements of scattered radiation within clouds, *J. Atm. Ocean. Technology*, *3*, 513–522, 1986.

Kite, A., The albedo of broken cloud fields, *Quart. J. Roy. Meteor. Soc.*, *113*, 517–531, 1987.

Lorenc, A.C., A global three-dimensional multivariate statistical interpolation scheme, *Mon. Wea. Rev.*, 701-721, 1981.

Le Treut, H., and Z. X. Li, Using Meteosat ISCCP data to validate a prognostic cloud generation scheme, *Atmosph. Res.*, *21*, 273–292, 1988.

Mc Clatchey, R. A., R. W. Fenn, J. E. A. Selby, F. E. Volz, and J. S. Garing, Optical properties of the atmosphere, *AFCRL–71–0279*, 85 pp., Air Force Cambridge Research Laboratories, Bedford, Mass., 1971.

Mc Kee, T. B., and S. K. Cox, Scattering of visible radiation by finite clouds, *J. Atmos. Sci.*, *31*, 1885–1892, 1974.

Morcrette, J. J., Infrared fluxes in stratiform clouds, *Beitr. Phys. Atmosph.*, *51*, 338–351, 1978.

Naber, P. S., and J. A. Weinman, The angular distribution of infrared radiances emerging from broken fields of cumulus clouds, *J. Geophys. Res.*, *89*, 1249–1257, 1984.

Neiburger, M., Reflexion, absorption and transmission of insolation by stratus clouds, *J. Meteor.*, *6*, 98–104, 1949.

Newiger, M., and K. Bahnke, Influence of cloud composition and cloud geometry on the absorption of solar radiation, *Beitr. Phys. Atmosph.*, *54*, 370–382, 1981.

Nicholls, S., The dynamics of stratocumulus aircraft observations and comparisons with a mixed layer model, *Quart. J. Roy. Meteor. Soc.*, *110*, 783–820, 1984.

Nicholls, S., and J. Leighton, An observational study of the structure of stratiform cloud sheets. Part I: Structure, *Quart. J. Roy. Meteor. Soc.*, *112*, 431–460, 1986.

O'Brien, D. M., Estimates for infrared transfer in finite clouds, *J. Atmos. Sci.*, *43*, 378–387, 1986.

Ohring, G., and P. Clapp, The effect of changes in cloud amount on the net radiation at the top of the atmosphere, *J. Atmos. Sci.*, *37*, 447–454, 1980.

Paltridge, G. W., Infrared emissivity, shortwave albedo and the microphysics of stratiform water clouds, *J. Geophys. Res.*, *79*, 4053–4058, 1974.

Parker, L., R. M. Welch, and D. J. Musil, Analysis of spatial inhomogeneities in cumulus clouds using high spatial resolution Landsat data, *J. Climate Appl. Meteor.*, *25*, 1301–1314, 1986.

Planck, V., The size distribution of cumulus in representative Florida populations, *J. Appl. Meteor.*, *8*, 46–57, 1969.

Platt, C. M. R., Infrared absorption and liquid water content in stratocumulus clouds, *Quart. J. Roy. Meteor. Soc.*, *102*, 533–561, 1976.

Phulpin, T., M. Derrien, and A. Brard, A two-dimensional histogram procedure to analyse cloud cover from the NOAA satellites high resolution imagery, *J. Climate Appl. Meteor.*, **22**, 1332-1345, 1983.

Preisendorfer, R. W., and G. L. Stephens, Multimode radiative transfer in finite optical media. I: fundamentals, *J. Atmos. Sci.*, *41*, 709–724, 1984.

Ramanathan, V., R. D. Cess, E. F. Harrison, P. Minnis, B. R. Barkstrom, E. Ahmad, and D. Hartmann, Cloud-radiative forcing and climate: Results from the Earth radiation budget experiment, *Science*, *243*, 1–140, 1989a,

Ramanathan, V., B. R. Barkstrom, and E. F. Harrison, Climate and the Earth's radiation budget, *Physics today*, *42*, 5, 22–32, 1989b.

Randall, D. A., J. A. Coakley, C. W. Fairall, R. A. Kropfli, and D. E. Lenschow, Outlook for research on subtropical marine stratiform clouds, *Bull. Amer. Meteor. Soc.*, *65*, 1290–1305, 1984.

Randall, D. A., J. A. Abeles and T. G. Corsetti, 1985: Seasonal simulations of the planetary boundary layer and boundary-layer stratocumulus clouds with a general circulation model. *J. Atmos. Sci.*, 42, 641-676.

Raschke, E., and K. D. Rockwitz, The International cirrus experiment ICE. Some preliminary results form the first field experiment, *Proc. Int. Rad. Symp.*, 6–9, 1988.

Reynolds, D. W., T. H. Vonder Haar, and S. K. Cox, The effect of solar radiation absorption in the tropical atmosphere, *J. Appl. Meteor.*, *14*, 433–444, 1975.

Rozenberg, G. V., V. N. Sinyyev, and A. G. Yantsen, Determination of the spectral characteristics of clouds from measurements of reflected solar radiation on the Kosmos 320 satellite, *Izv. Acad. Sci. USSR Atmos. Oceanic Phys.*, Engl. Transl., *10*, 7–14, 1974.

Sasamori, T., A statistical model for stationary atmospheric cloudiness, liquid water content, and rate of precipitation, *Mon. Wea. Rev.*, **103**, 1037-1049, 1975.

Schiffer, R. A., and W. B. Rossow, The International Satellite Cloud Climatology Project (ISCCP) the first project of the World Climate Research Programme, *Bull. Amer. Meteor. Soc.*, *64*, 779–784, 1983.

Starr, D. O'C., A cirrus cloud experiment: intensive field observations planned for FIRE, *Bull. Amer. Meteor. Soc.*, *68*, 119–124, 1987.

Schlesinger, M. E., and J. F. B. Mitchell, Model projections of equilibrium climatic response to increased CO_2 concentration, in *Projecting the climatic effects of increasing carbon dioxide*, edited by M. C. Mc Cracken and F. M. Luther, US Dept. of Energy, Washington D. C., USA, 1986.

Schmetz, J., On the parameterization of the radiative properties of broken clouds, *Tellus*, *36A*, 417–432, 1984.

Schubert, W. H., W. S. Wakefield, E. J. Steiner, and S. K. Cox, Marine stratocumulus convection. Part I: Governing equations and horizontally homogeneous solutions, *J. Atmos. Sci., 36*, 1286–1307, 1979.

Slingo, A., R. Brown, and C.L. Wrench, A field study of nocturnal stratocumulus. III: High resolution radiative and microphysical observations, *Quart. J. Roy. Meteor. Soc., 108*, 145–165, 1982a.

Slingo, A., S. Nicholls, and J. Schmetz, Aircraft observations of marine stratocumulus during JASIN, *Quart. J. Roy. Meteor. Soc., 108*, 833–856, 1982b.

Slingo, A., and H. M. Schrecker, On the shortwave radiative properties of stratiform water clouds, *Quart. J. Roy. Meteor. Soc., 108*, 407–426, 1982.

Slingo, J.M., 1987: The development and verification of a cloud prediction scheme for the ECMWF model. *Quartely J. Roy. Meteor. Soc.*, 113, 899-927.

Slingo, J.M., 1987: Clouds in extended range forecast models. in Clouds in Climate II, a WCRP workshop on Modeling and Observations (Columbia, Maryland, October 19-23, 1987) available from NASA.

Somerville, C. J., and L. A. Remer, Cloud optical thickness feedbacks in the CO_2 climate problem, *J. Geophys. Res., 89*, 9668–9672, 1984.

Stephens, G. L., Radiation profiles in extended water clouds. I: Theory, *J. Atmos. Sci., 35*, 2111–2122, 1978a.

Stephens, G. L., Radiation profiles in extended water clouds. II: Parametrization schemes, *J. Atmos. Sci., 35*, 2123–2132, 1978b.

Stephens, G. L., G. W. Paltridge, and C. M. R. Platt, Radiation profiles in extended water clouds. III: Observations, *J. Atmos. Sci., 35*, 2133–2141, 1978.

Stephens, G. L., Optical properties of eight water cloud types, *CSIRO Aust. Div. Atmos. Phys., Tech. pap. No 36*, 35 pp, 1979.

Stephens, G.L., and C.M.R. Platt, Aircraft observations of the radiative and microphysical properties of stratocumulus and cumulus cloud fields, *J. Climate Appl. Meteor., 26*, 1243–1269, 1987.

Stephens, G. L., and J. C. Scott, A high speed spectrally scanning radiometer(SPERAD) for airborne measurements of cloud optical properties, *J. Atmos. Oc. Tech., 2*, 148-156, 1985.

Stephens, G. L., and P. J. Webster, Cloud decoupling of the surface and planetary radiative budgets, *J. Atmos. Sci., 41*, 681–686, 1984.

Sundqvist, H., A parameterization scheme for non-convective condensation including prediction of cloud water content, *Quart. J. Roy. Meteor. Soc., 104*, 677–690, 1978.

Sundqvist, H., Inclusion of cloud liquid water as a prognostic variable, *Proc. ECMWF Workshop on Cloud cover parameterization in numerical models*, Reading, UK, 26–28 Nov., 1984.

Twomey, S., The influence of pollution on the shortwave albedo of clouds, *J. Atmos. Sci., 34*, 1149–1152, 1977.

Twomey, S., and C. F. Bohren, Simple approximations for calculations of absorption in clouds, *J. Atmos. Sci., 37*, 2086–2094, 1980.

Van de Hulst, H. C., *Light scattering by small particles*, 470 pp., John Wiley, New York, 1957.

Webster, P. J., and G. L. Stephens, Cloud-radiation interaction and the climate problem, in *The gobal climate*, edited by J. Houghton, Cambridge University Press, Cambridge, UK, 1984.

Welch, R. M., and B. A. Wielicki , Stratocumulus cloud field reflected fluxes: The effect of cloud shape, *J. Atmos. Sci., 41*, 3085–3103, 1984.

Welch, R. M., and B. A. Wielicki, A radiative parametrization of stratocumulus cloud fields, *J. Atmos. Sci., 42*, 2888–2897, 1985.

Welch, R. M., and B. A. Wielicki, The stratocumulus nature of fog, *J. Climate Appl. Meteor., 25*, 101–111, 1986.

Welch, R. M., and W. G. Zdunkowski, The effect of cloud shape on radiative characteristics, *Beitr. Phys. Atmosph., 54*, 482–491, 1981.

Wielicki, B. A., and R. M. Welch, Cumulus cloud properties derived using LANDSAT satellite data. *J. Climate Appl. Meteor., 25*, 261–276, 1986.

Wiscombe, W.J., R.M. Welch, and W.D. Hall, The effects of very large drops on cloud absorption. Part I: Parcel models, *J. Atmos. Sci., 41*, 1336–1355, 1984.

Wiscombe, W., and R. Welch, Reply to a comment on "The effects of very large drops on cloud absorption" by Hegg, *J. Atmos. Sci., 43*, 401–407, 1986.

Woods, J. D., The upper ocean and air-sea interaction in climate, in *The gobal climate*, edited by J. Houghton, Cambridge University Press, Cambridge, UK, 1984.

World Climate Programme (WCP), *A preliminary cloudless standard atmosphere for radiation computation*, WCP-112, 53 pp., Radiation Commission, Boulder, Co, USA, 1986.

Yamamoto, G., M. Tanaka, and M. Asano, Radiative transfer in water clouds in the infrared region, *J. Atmos. Sci., , 27*, 282–292, 1970.

Figure captions

Figure 1: Spatial extension of the NEPHOS file. Satellite data are received for the area surrounded by dashes, large-scale fields analyzed at ECMWF are stored for the area enclosed by the dotted line. Visual nephanalysis is performed on Meteosat data for the area within the thick full line.

Figure 2: Observed cloud covers and associated analysed relative humidities RH for a subset of low-level clouds (see section 2).

Figure 3: Observed cloud covers and associated variation of potential temperature in the lower atmosphere for the same subset as Figure 3.

Figure 4: The mean profile of cumulative cloud cover derived from satellite observations (full line with dots), calculated with the original RH-scheme including (full line) or without (dashed line) the θ-filter.

Figure 5 : Comparison between measured reflectances R and transmittances T and calculated ones using : (a), the simple parameterization described in section 3.1; (b), more detailed computations by the authors of the referenced papers listed in Table 3. The squares (□) refer to the reflectances, the crosses + refer to the transmittances.

Figure 6: . Same as Figure 5 but for cloud absorption.

Figure 7 : Liquid water content w and drop effective radius r_e as a function of the h[illegible] above the cloud base (simulation of the NEPHOS experiment).

Figure 8 : Variation of the absorptance with the cloud thickness or, equivalently, the liquid water path for the cloud described in section 2.2, for two values of the solar zenith angle (a) $\theta_o = 66°$ and (b) $\theta_o = 37°$. Three cases are considered: the clear air absorptance of the layer in which the cloud is located (○) and the cloud layer absorptance without ( ) and with (○) the cloud drop absorption.

Figure 9 : Variation of the additional absorptance due to the interstitial aerosols, for two values of the solar zenith angle (a) $\theta_o = 66°$ and (b) $\theta_o = 37°$. Three types of aerosols are considered: maritime(○), continental (□) and urban-industrial (△). The full lines refer to the cloud absorptance while the dashed lines refer to the clear absorptance.

Figure 10 : Horizontal extension of a typical cloud observed during the NEPHOS experiment.

Figure 11 : Time variations (10 sec. smoothed) of the shortwave fluxes recorded during a descent throught the stratocumulus described on Figure 10.

Figure 12 : Spectral reflectance above a stratocumulus cloud located between 250 and $550m$. The liquid water optical thickness is $\delta = 20$; r_e is the drop effective radius, and δ_a the aerosol optical thickness under the cloud top height.

Figure 13 : Summary of vertical profiles corresponding to a stratocumulus observed during the NEPHOS experiment:
(a) Liquid water content.
Two idealized profiles are reported, one including the cloud top roll, the other one excluding them.
(b) Longwave radiative fluxes.
Observations are compared to the results of parameterization (26) for the two idealized profiles; the stars correspond to the results of calculations taking scattering into account.
(c) Infrared cooling rate.

Figure 14 : The influence of broken cloud fields on the infrared radiation lost to space, illustrated by the behavior of the effective cloud cover A_ϵ as a function of A_c. Results are for a regular array of cuboïdal clouds. Different cloud aspect ratios are considered. From Harshvardhan (1982).

Figure 15 : Schematic representation: (a), of an isolated cloud and an equivalent plan-parallel cloud fraction; (b), of a broken cloud field and its plan-parallel counterpart.

Figure 16 : The albedo effect of broken cloud fields for solar radiation, illustrated by the behavior of A_ϵ/A_c (where A_ϵ is the effective cloud cover). Results are for a regular array of cuboïdal clouds. Differend cloud aspects ratios (a = 0.5, 1, 2) and two zenith angles ($\theta_o = 0°$ and $60°$) are considered. From Welch and Wielecki (1984).

Table 1: statistical analysis of satellite derived cloud cover and analysed large scale fields : vertical profile (from Heinburger and Royer, private communication)

Selection : RH, RH^2, RH^3,G, G^2, G^3,W, R_i,dT/dz, dq/dz.
Period : Sept. 1, oct. 30 1982: 80 278 cases.

Parameter	Multiple Correlation Coefficient	Correlation Coefficient $r(X(z), A_c(z))$
X		
RH^2	.651	.651
G(Geopotential)	.672	-.582
dT/dz	.699	-.219
W	.709	-.25
G^2	.719	-.465
dq/dz	.730	-.390

Application of the multiple regression to the data set: $\sigma \simeq 0.25$

Initially (Geleyn) $\sigma \simeq 0.35$

Table 2: Mean values of the parameters of the radiation budget at the top of the atmosphere deduced by Buriez et al. (1988) for the area of Figure 1 and a full year of observations (feb 82-feb 83). The calculated values are for the model generated cloud covers (ECMWF model, version 1982). A_C is the cloud cover, α_1 the albedo in AVHRR channel 1 (0.5 0.7 μm), Q is the absorbed shortwave radiation, $T_{10.5}$ is the radiative temperature in AVHRR channel 4, F is the outgoing longwave flux, and R_N is the radiation budget.

Parameter	unit	Observed	Calculated
A_C		0.602	0.340
α_1		0.295	0.217
Q	Wm^{-2}	242	265
$T_{10.5}$	K	272	281
F	Wm^{-2}	233	249
R	Wm^{-2}	9	16
$\frac{\partial \alpha_1}{\partial A_C}$		0.389	0.459
$\frac{\partial Q}{\partial A_C}$	Wm^{-2}	-108	123
$\frac{\partial F}{\partial A_C}$	Wm^{-2}	- 50	- 40
$\frac{\partial R}{\partial A_C}$	Wm^{-2}	- 58	83

Table 3 : SW RADIATION OBSERVATIONS IN THE LOW EXTENDED CLOUDS SINCE 1970.

The measured reflectances R, transmittances T and absorptances Abs (Abs_{cor} refers to Ackerman and Cox (1982) method) are compared to theoretical values (a) obtained by the authors (b)derived from the liquid water path W, the cloud depth ΔZ, the solar zenith angle θ_o and the surface reflectivity ρ_s, by using the method described in section 2.1.

Authors	Lat	W (g/m^2)	ΔZ (m)	θ_0	ρ_s	measured R %	measured T %	measured Abs %	measured Abs_{cor} %	calculated (a) R %	calculated (a) T %	calculated (a) Abs %	calculated (b) R %	calculated (b) T %	calculated (b) Abs %
Paltridge (1971)	17S		560			42		2							
	"		180			26		0							
	"		410			38		2							
Paltridge (1974)	31S	75	650	10°	0.12	50	58	0					61	36	8
	"	90	840	35°	"	59	40	6					68	27	7
Binenko et al. (1975)		25	100	39°	-	27	72	1		30	63	7	33	64	4
		75	300	74°	-	65	24	11		66	27	7	73	23	4
		100	450	26°	-	59	36	5		56	32	12	64	29	7
		125	550	50°	-	66	19	15		69	18	13	73	20	6
		450	1900	54°	-	71	9	20		77	8	15	84	4	12
Reynolds et al. (1975)	14N			11°		42	46	12							
	15N			19°		37	27	36							
	16N			16°		37	41	22							
Herman (1977)	72N		100 to 900	54° to 67°	0.53 to 0.63	60 to 75	46 to 86	3 to 12	1 to 6						
Stephens et al. (1978)	37S	52	320	36°	0.55	67	51	5		67	50	11	65	60	8
	"	29	230	31°	0.18	50	54	4		44	59	8	44	62	5
	"	32	180	39°	0.30	49	67	6		44	69	8	51	62	6
	42S	52	400	75°	0.00	68	12	20		65	32	3	71	25	4
	"	61	480	72°	"	75	12	14		76	19	6	72	23	4
	"	68	550	62°	"	65	21	14		68	24	8	70	19	5
Schmetz et al. (1981)	60N	110	350	45°	0.08	68	29	6		64	33	5	68	28	6
	59N	105	370	50°	"	68	35	4		64	34	5	69	27	6
Slingo et al. (1982)	60N	150	435	44°	0.05	68	27	7		68 to 71	24 to 30	4 to 9	72	22	7
Ackerman and Cox (1982)	20N							18	9						
								10	5						

Table 3 *(continued)*

Authors	*Lat*	W (g/m^2)	ΔZ (m)	θ_0	ρ_s	measured R %	measured T %	measured Abs %	measured Abs_{cor} %	calculated (a) R %	calculated (a) T %	calculated (a) Abs %	calculated (b) R %	calculated (b) T %	calculated (b) Abs %
Bonnel et al. (1983)	49N		530	42°	0.07	65	32	5							
	"		900	57°	"	53	40	10							
	"		1300	65°	"	61	57	-14							
	"		1600	54°	"	82	8	11							
	"		1800	57°	"	55	51	-2							
	5N		1400	19°	"	48	63	-7							
Herman and Curry (1984)	74N	11	235	51°	0.70	55	69	23	-1	61	86	3	70	84	4
	74N	32	410	52°	0.70	79	80	1	-2	66	71	5	73	66	7
	74N	53	202	54°	0.57	59	60	15	3	70	57	4	69	55	7
	72N	43	226	56°	0.55	63	55	17	8	69	62	5	69	55	6
	75N	7	176	51°	0.58	57	70	15	-4	71	87	2	61	86	3
	73N	17	436	57°	0.47	49	71	12	4	59	79	2	61	65	5
	77N	117	380	54°	0.57	74	43	7	4	79	40	6	76	38	7
	78N	70	256	55°	0.56	80	66	-5	-4	78	50	6	72	48	7
	78N	61	292	57°	0.58	67	57	8	4	76	54	5	73	49	7
	78N	72	321	57°	0.55	72	50	6	5	74	50	4	73	44	7
	77N	53	283	57°	0.58	66	48	12	-1	76	52	4	72	51	7
	72N	15	791	54°	0.57	59	49	23	5	65	71	4	64	72	5
Nicholls (1984)	55N	81	450	35°	0.05	63	31	7		65	28	8	63	32	7
Nicholls and Leighton (1986)	55N	68	320	44°	0.06	66	31	7		69	27	5	61	35	6
	54N	148	450	35°	0.05	62	31	8		65	28	8	70	24	7
	55N	32	190	36°	0.05	44	62	-1		41	58	4	43	55	5
	50N	138	670	75°	0.06	79	33	-9		68	28	6	82	13	5
Hignett (1987)	56N	34 to 56	187 to 237	34°	0.08	43 to 60				43 to 55			46 to 53		
Stephens and Platt (1987)	17S			40°		39		8		43		5			
Foot (1988)	49N	225	1005	61°	0.11	80 to 82		10 to 15		82		7	83		8
NEPHOS exp.	49N	22	190	66°	0.07	74	36			53	48		53	47	
	"	to			"	and				to	to		to	to	
	"	90	325		"	76				73	23		72	24	

Table 4: Dependence of the shortwave cloud absorptance Abs on the effective radius r_e

$W = 2.5\ gm^{-2}$

$r_e(\mu m)$	3.8	↗	9.6
$Abs(\theta_0 = 66°)$	0.73%	↘	0.66%
$Abs(\theta_0 = 37°)$	0.62%	↘	0.46%

$W = 250\ gm^{-2}$

$r_e(\mu m)$	3.8	↗	9.6
$Abs(\theta_0 = 66°)$	4.5%	↗	6.4%
$Abs(\theta_0 = 37°)$	5.9%	↗	8.1%

Table 5: Shortwave cloud absorptances (Abs) calculated for the case of Fig. 22.

Upper leg	Lower leg	Apparent Absorptance (%) $\theta_0 = 66°$	Corrected Absorptance (%) $\theta_0 = 66°$	Apparent Absorptance (%) $\theta_0 = 37°$	Corrected Absorptance (%) $\theta_0 = 37°$
t_1	b_1	2.5	2.5	2.9	2.9
t_2	b_2	4.8	4.8	6.1	6.1
t_1	b_2	22.8	2.3	29.2	3.9
t_2	b_1	-15.3	4.6	-19.8	4.6

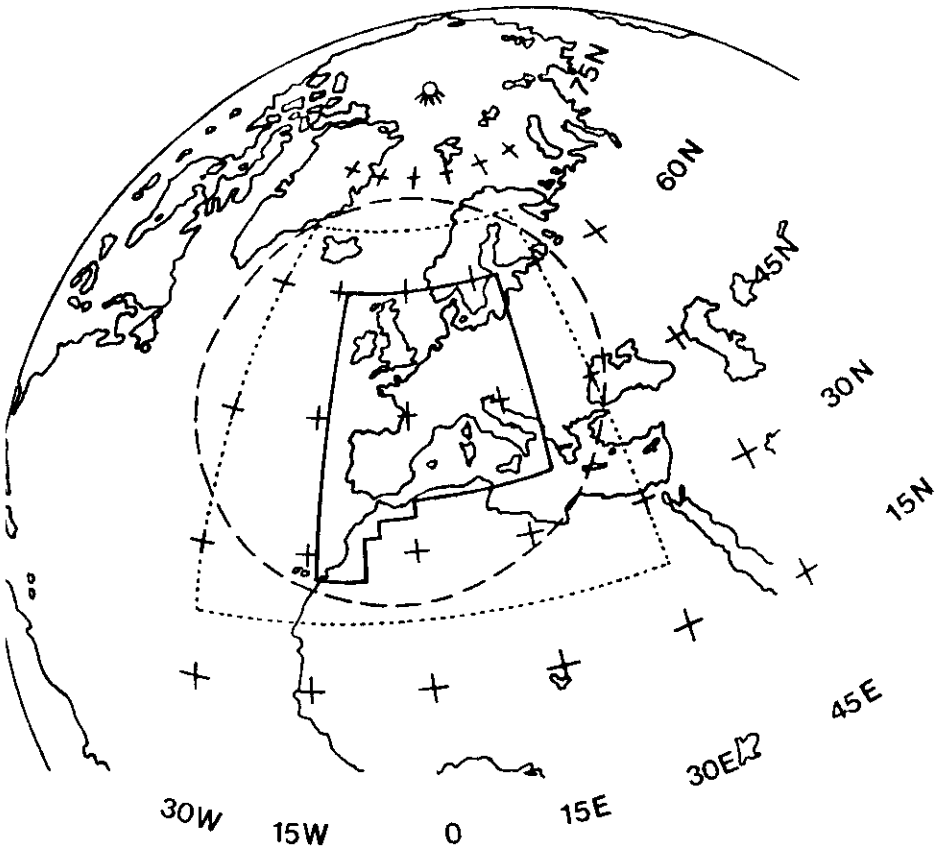

1437 cases with no cloud above 800 mb

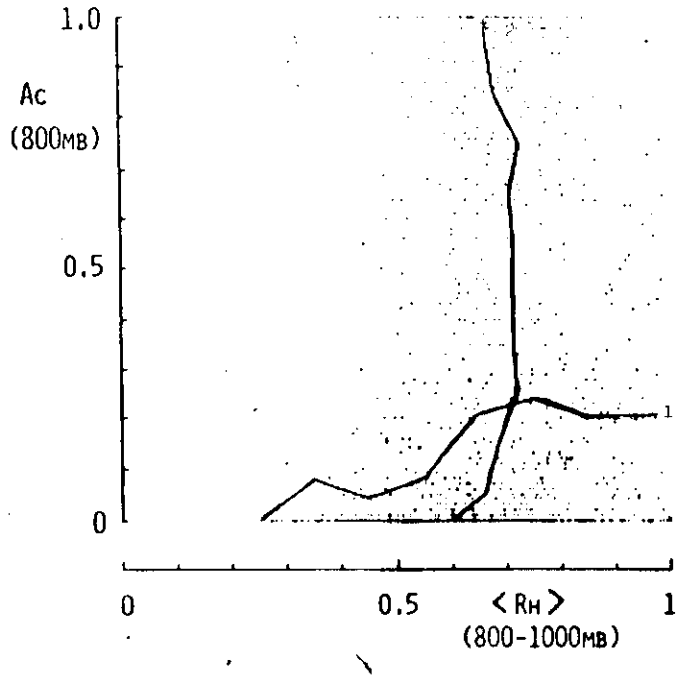

1 - Averaged cloud cover as function of relative humidity (R_H)

2 - Averaged R_H as function of cloud cover

1437 cases with no cloud above 800 mb

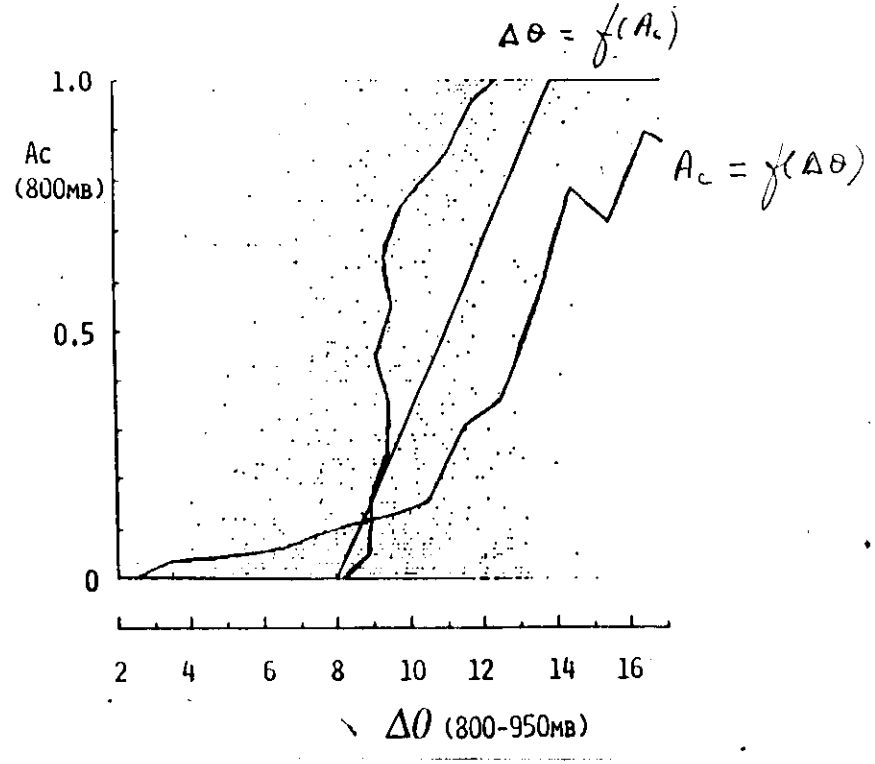

For the whole data set (1866 cases)

- no bias at 800 mb
- root-mean square r_{ms} = 0.34

original (Geleyn) scheme : r_{ms} = 0.41
bias = 0.18

Fig 2

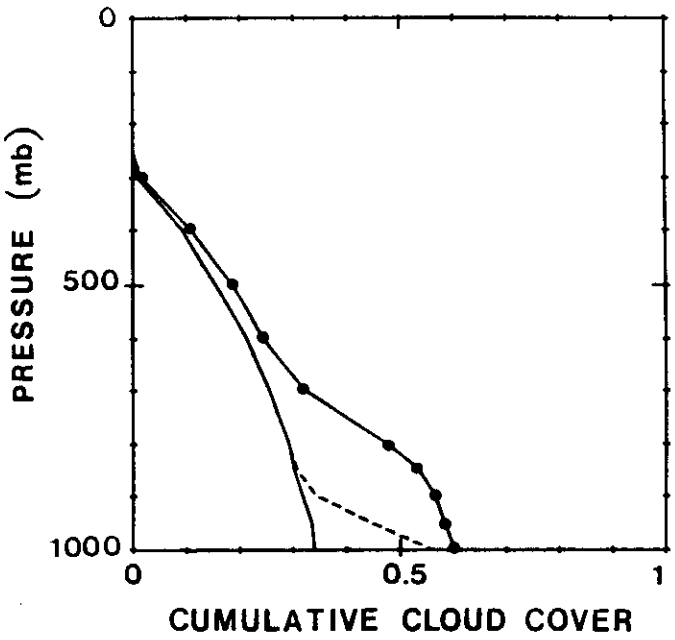

Figure 4

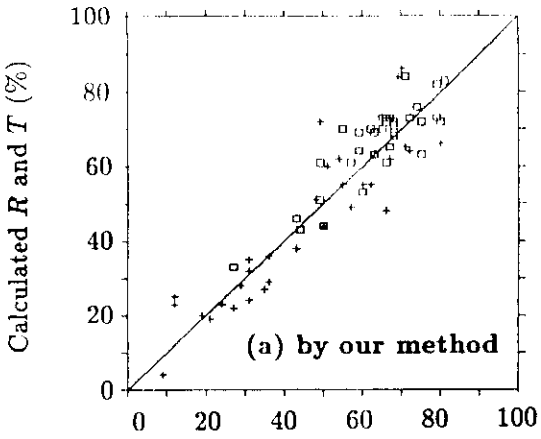
Calculated R and T (%)
(a) by our method
0
20
40
60
80
100

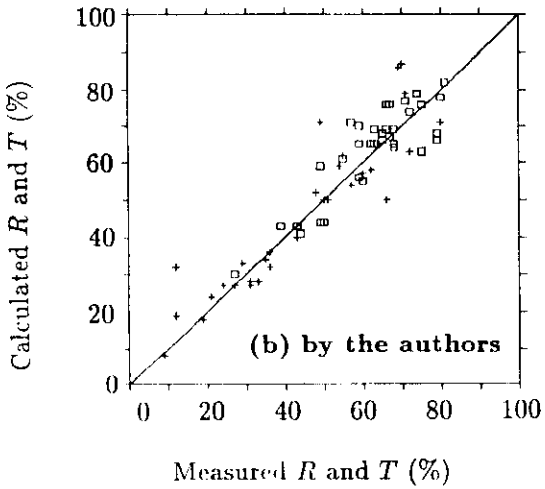
Calculated R and T (%)
(b) by the authors
Measured R and T (%)
0
20
40
60
80
100

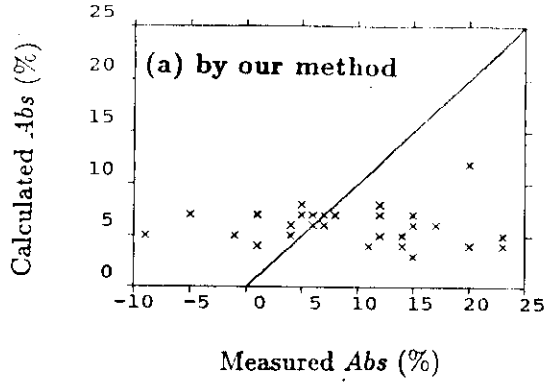
Calculated *Abs* (%)
(a) by our method
Measured *Abs* (%)
-10
-5
0
5
10
15
20
25

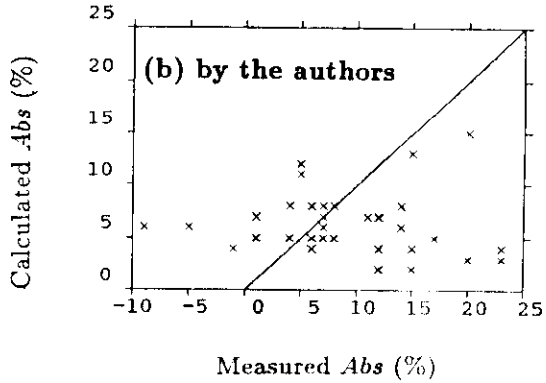
Calculated *Abs* (%)
(b) by the authors
Measured *Abs* (%)
-10
-5
0
5
10
15
20
25

(b)

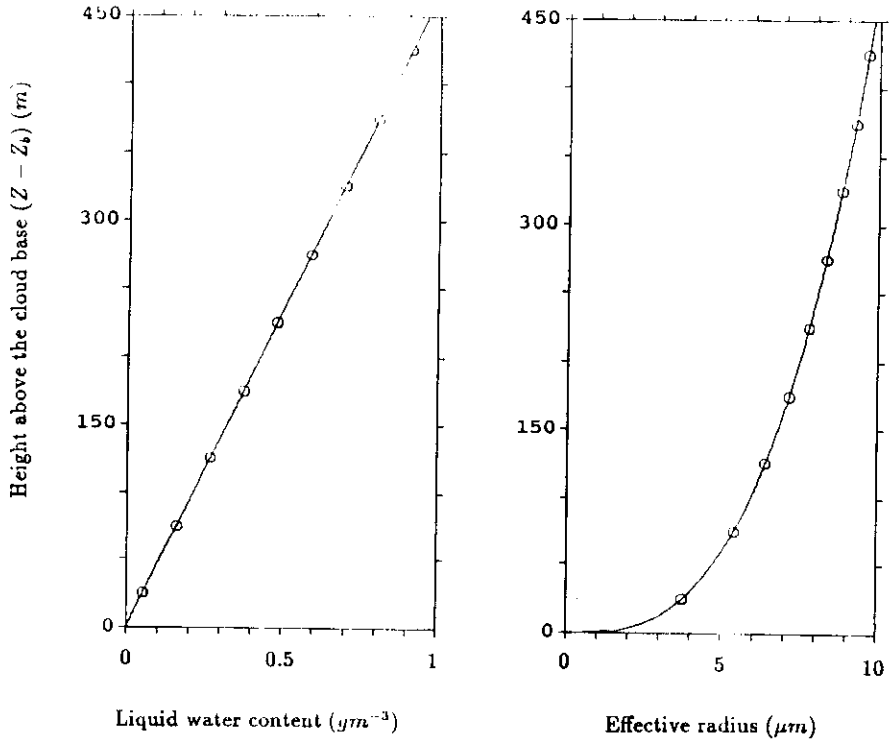
Height above the cloud base $(Z - Z_b)$ (m)
450
300
150
0
0
0.5
1
Liquid water content (gm^{-3})
450
300
150
0
0
5
10
Effective radius (μm)

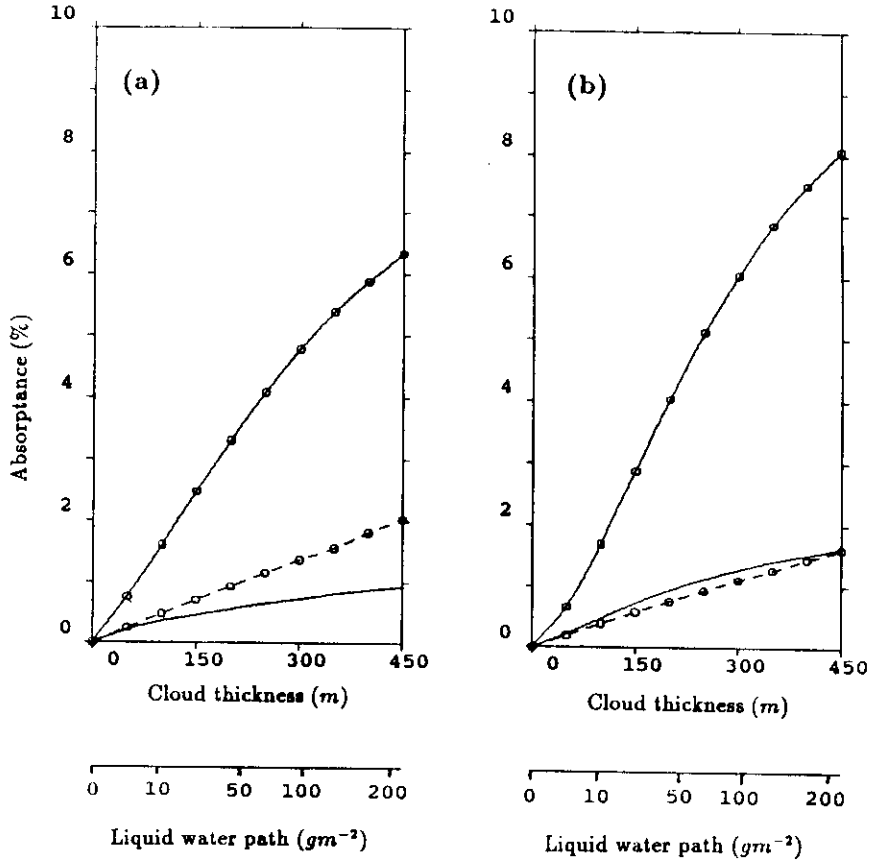
Absorptance (%)
10
8
6
4
2
0
(a)
0
150
300
450
Cloud thickness (m)
0
10
50
100
200
Liquid water path (gm^{-2})
(b)
Cloud thickness (m)
Liquid water path (gm^{-2})

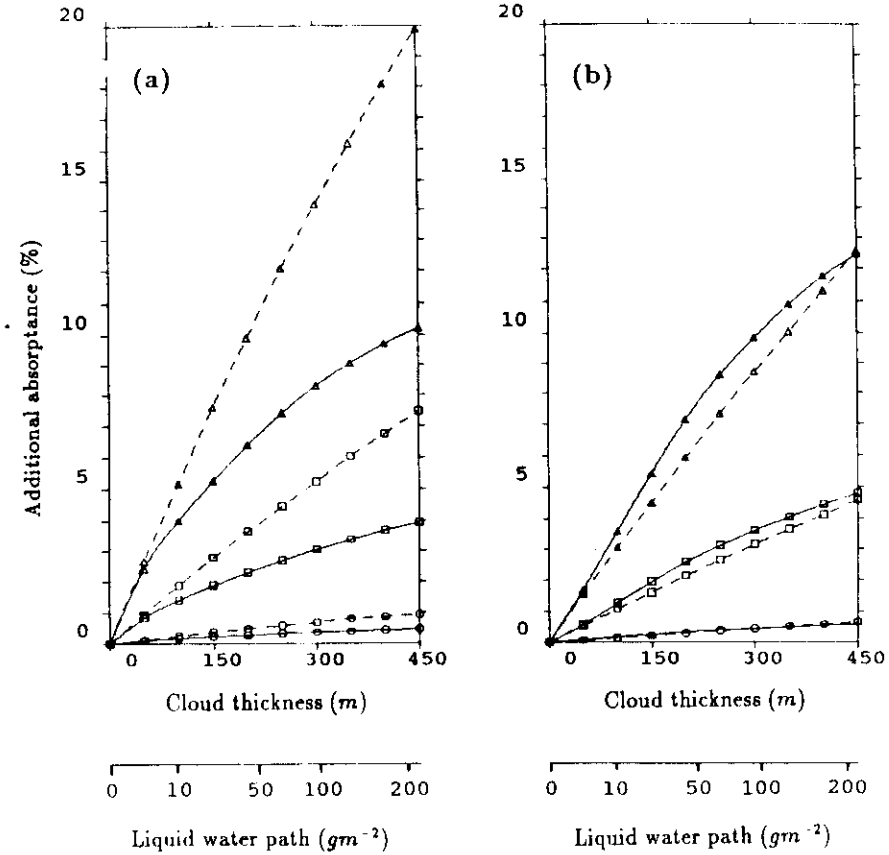
(a)
(b)
Additional absorptance (%)
0
5
10
15
20
0
150
300
450
Cloud thickness (m)
0
10
50
100
200
Liquid water path (gm^{-2})

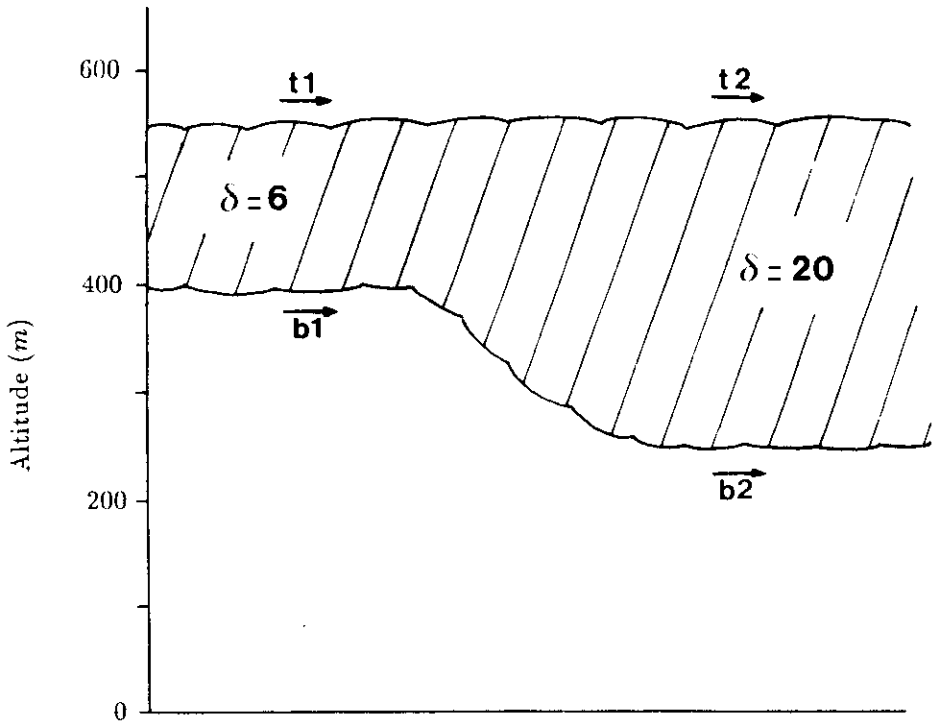
Altitude (m)
600
400
200
0
t1
t2
b1
b2
δ = 6
δ = 20

Fig 4a

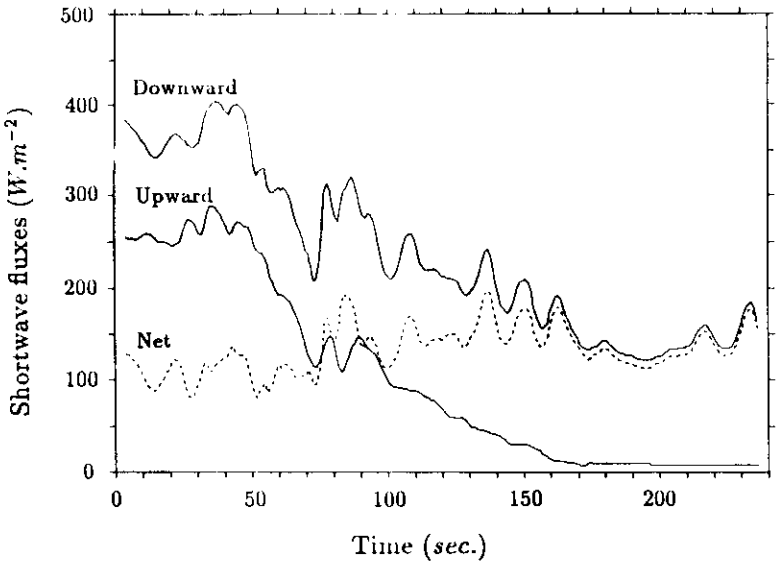
Downward
Upward
Net
Shortwave fluxes ($W.m^{-2}$)
Time ($sec.$)
500
400
300
200
100
0
0
50
100
150
200

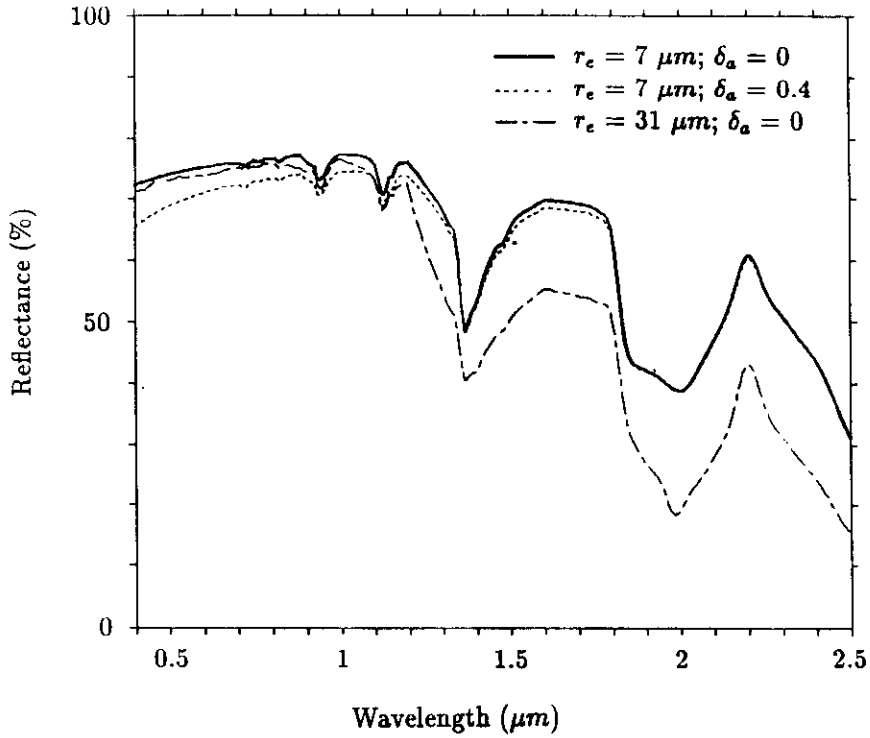
$r_e = 7\ \mu m;\ \delta_a = 0$
$r_e = 7\ \mu m;\ \delta_a = 0.4$
$r_e = 31\ \mu m;\ \delta_a = 0$
Reflectance (%)
Wavelength (μm)
100
50
0
0.5
1
1.5
2
2.5

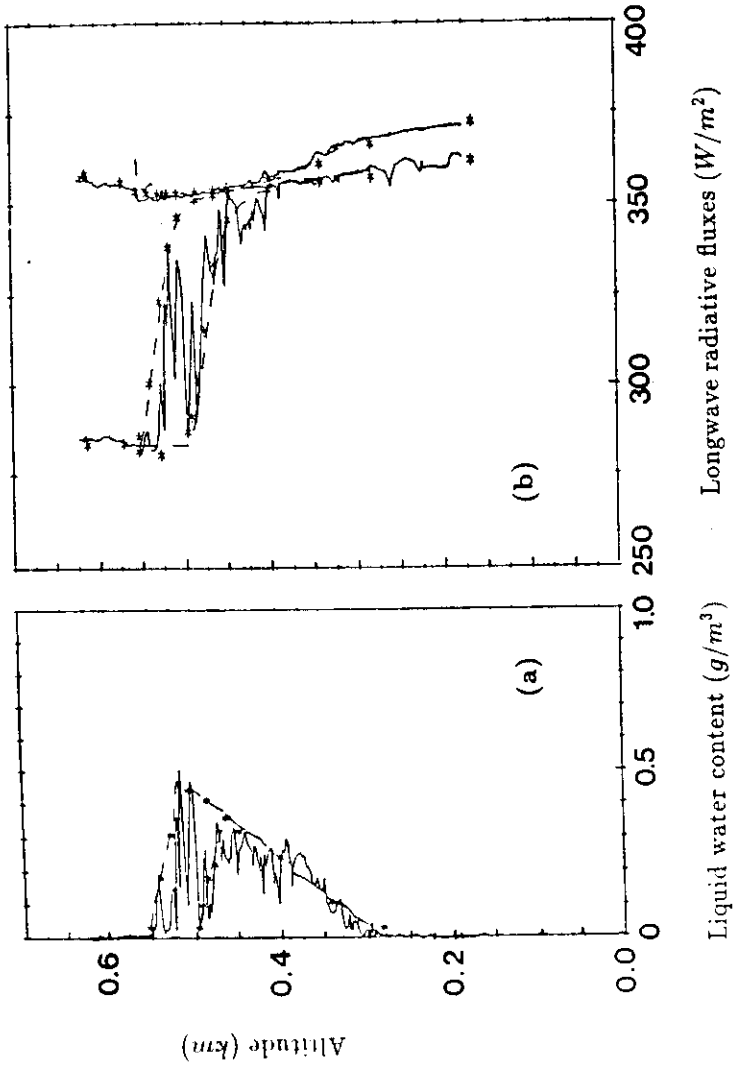
400
350
300
250
(b)
Longwave radiative fluxes (W/m^2)
1.0
0.5
0
(a)
Liquid water content (g/m^3)
0.6
0.4
0.2
0.0
Altitude (km)

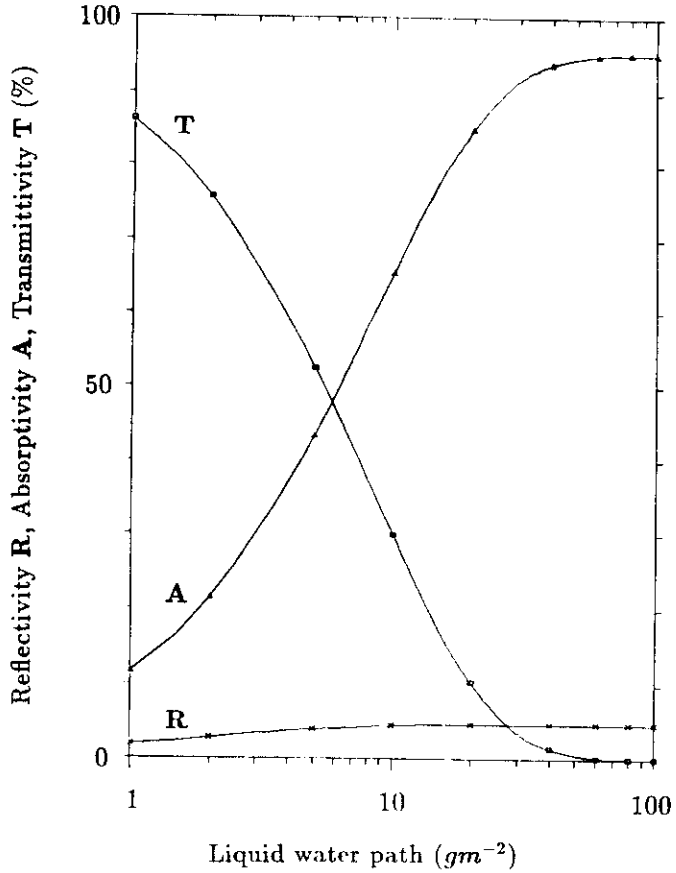
100
50
0
T
A
R
1
10
100
Reflectivity R, Absorptivity A, Transmittivity T (%)
Liquid water path (gm^{-2})

14

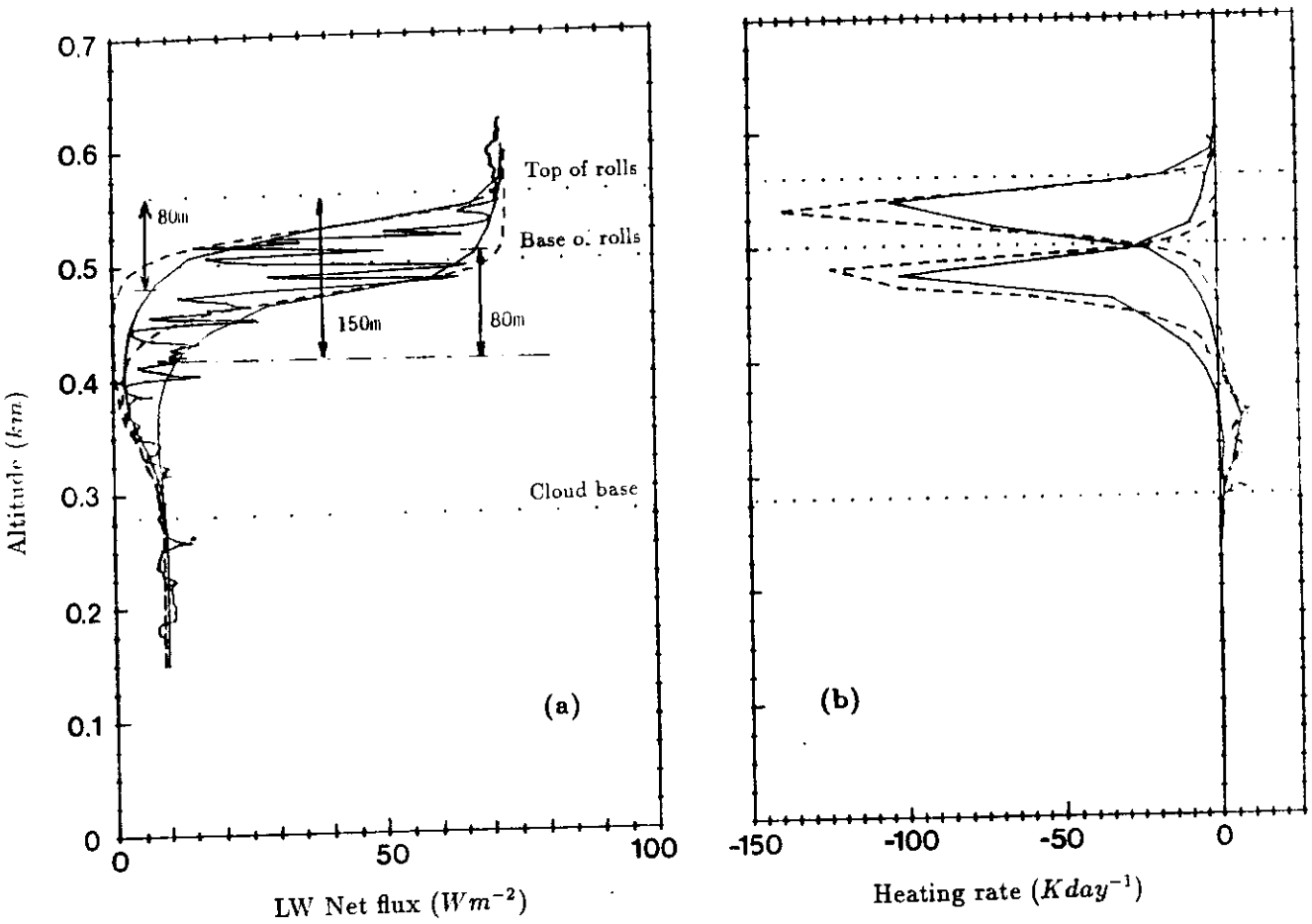
Altitude (km)
0.7
0.6
0.5
0.4
0.3
0.2
0.1
0
80m
150m
80m
Top of rolls
Base of rolls
Cloud base
(a)
0
50
100
LW Net flux (Wm^{-2})
(b)
-150
-100
-50
0
Heating rate ($Kday^{-1}$)

Fig 2

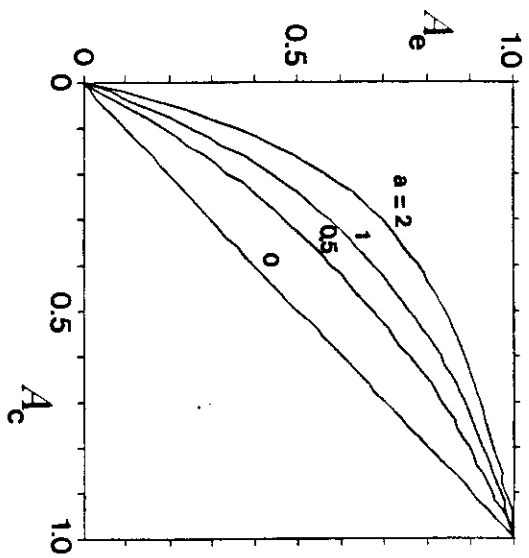
A_e
0
0.5
1.0
A_c
0
0.5
1.0
a = 2
1
0.5
0

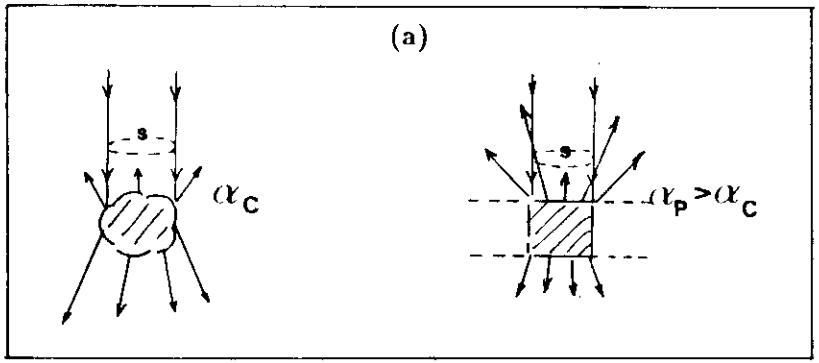
(a)
s
α_C
s
$\alpha_P > \alpha_C$

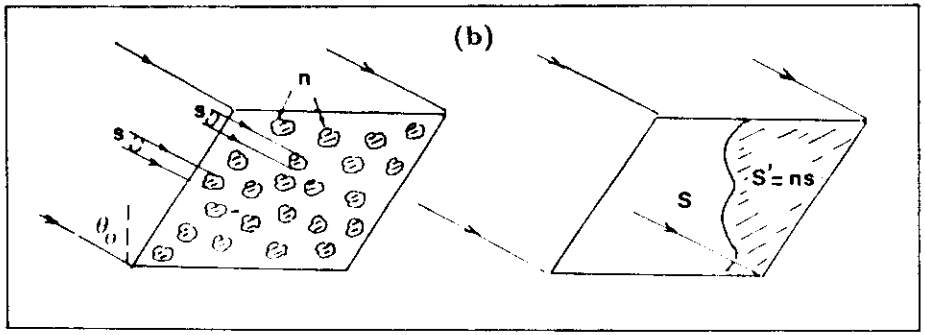
(b)
n
s
s
θ_0
S
S' = ns

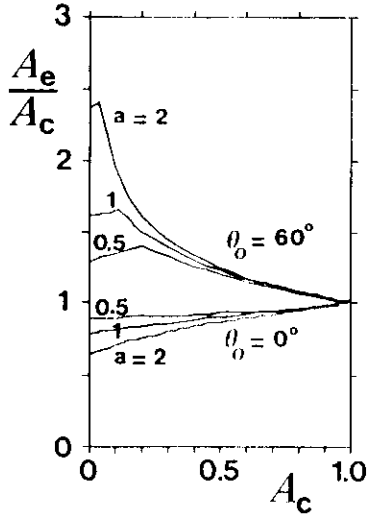
$\frac{A_e}{A_c}$
3
2
1
0
a = 2
1
0.5
θ_0 = 60°
0.5
1
a = 2
θ_0 = 0°
0
0.5
1.0
A_c